CERN-TH-2017-102

CERN-LPCC-2017-02
FERMILAB-PUB-17-152-T
IPPP/17/38
ZU–TH 12/17

Precise predictions for V+jets dark matter backgrounds

J. M. Lindert[1], S. Pozzorini[2], R. Boughezal[3], J. M. Campbell[4], A. Denner[5], S. Dittmaier[6], A. Gehrmann-De Ridder[2,7], T. Gehrmann[2], N. Glover[1], A. Huss[7], S. Kallweit[8], P. Maierhöfer[6], M. L. Mangano[8], T.A. Morgan[1], A. Mück[9], F. Petriello[3,10], G. P. Salam[*8], M. Schönherr[2], and C. Williams[11]

[1] *Institute for Particle Physics Phenomenology, Department of Physics, University of Durham, Durham, DH1 3LE, UK*
[2] *Physik-Institut, Universität Zürich, Winterthurerstrasse 190, CH-8057 Zürich, Switzerland*
[3] *High Energy Physics Division, Argonne National Laboratory, Argonne, IL 60439, USA*
[4] *Fermilab, P.O.Box 500, Batavia, IL 60510, USA*
[5] *Universität Würzburg, Institut für Theoretische Physik und Astrophysik, 97074 Würzburg, Germany*
[6] *Albert-Ludwigs-Universität Freiburg, Physikalisches Institut, 79104 Freiburg, Germany*
[7] *Institute for Theoretical Physics, ETH, CH-8093 Zürich, Switzerland*
[8] *Theoretical Physics Department, CERN, CH-1211 Geneva 23, Switzerland*
[9] *Institut für Theoretische Teilchenphysik und Kosmologie, RWTH Aachen University, D-52056 Aachen, Germany*
[10] *Department of Physics & Astronomy, Northwestern University, Evanston, IL 60208, USA*
[11] *Department of Physics, University at Buffalo, The State University of New York, Buffalo 14260 USA*

Abstract

High-energy jets recoiling against missing transverse energy (MET) are powerful probes of dark matter at the LHC. Searches based on large MET signatures require a precise control of the $Z(\nu\bar{\nu})+$ jet background in the signal region. This can be achieved by taking accurate data in control regions dominated by $Z(\ell^+\ell^-)+$ jet, $W(\ell\nu)+$ jet and $\gamma+$ jet production, and extrapolating to the $Z(\nu\bar{\nu})+$ jet background by means of precise theoretical predictions. In this context, recent advances in perturbative calculations open the door to significant sensitivity improvements in dark matter searches. In this spirit, we present a combination of state-of-the-art calculations for all relevant $V+$ jets processes, including throughout NNLO QCD corrections and NLO electroweak corrections supplemented by Sudakov logarithms at two loops. Predictions at parton level are provided together with detailed recommendations for their usage in experimental analyses based on the reweighting of Monte Carlo samples. Particular attention is devoted to the estimate of theoretical uncertainties in the framework of dark matter searches, where subtle aspects such as correlations across different $V+$ jet processes play a key role. The anticipated theoretical uncertainty in the $Z(\nu\bar{\nu})+$ jet background is at the few percent level up to the TeV range.

[*] on leave from CNRS, UMR 7589, LPTHE, F-75005, Paris, France

Contents

1 Introduction

The signature of missing transverse energy (MET) is one of the most powerful tools in the interpretation of data from hadron colliders. In the Standard Model (SM), MET arises from the neutrinos from the decay of W and Z bosons, and it can be used in their identification and study, as well as in the identification and study of Higgs bosons, top quarks and other SM particles whose decay products include W or Z bosons. But MET is also an almost omnipresent feature of theories beyond the SM (BSM), where it can be associated to the decay of new particles to W and Z bosons, or directly to the production of new stable, neutral and weakly interacting particles. Typical examples are theories with dark matter (DM) candidates, or Kaluza-Klein theories with large extra dimensions. Depending on the details, MET is accompanied by other model-discriminating features, such as the presence of a small or large multiplicity of hard jets, or of specific SM particles. The experimental search for these extensions of the SM relies on a proper modeling of the SM backgrounds to the MET signature. The determination of these backgrounds is ideally done by using data control samples, but theoretical input is often helpful, or even necessary, to extend the experimental information from the control to the signal regions, or to extend the application range of the background predictions and to improve their precision [1–3].

In this paper we focus on the theoretical modeling of the SM $V+$jet backgrounds to inclusive production of large MET recoiling against one or more hadronic jets. These final states address a broad set of BSM models, where the production of an otherwise invisible final state is revealed by the emission of one or more high-p_{T} jets from initial state radiation, where p_{T} is the momentum in the transverse plane.[1] Recent publications by ATLAS [5] and CMS [6, 7], relative to LHC data collected at $\sqrt{s} = 13\,\mathrm{TeV}$, document in detail the current experimental approaches to the background evaluation. The leading background is

[1] For a recent comprehensive review of DM models leading to this class of signatures, see e.g. [4].

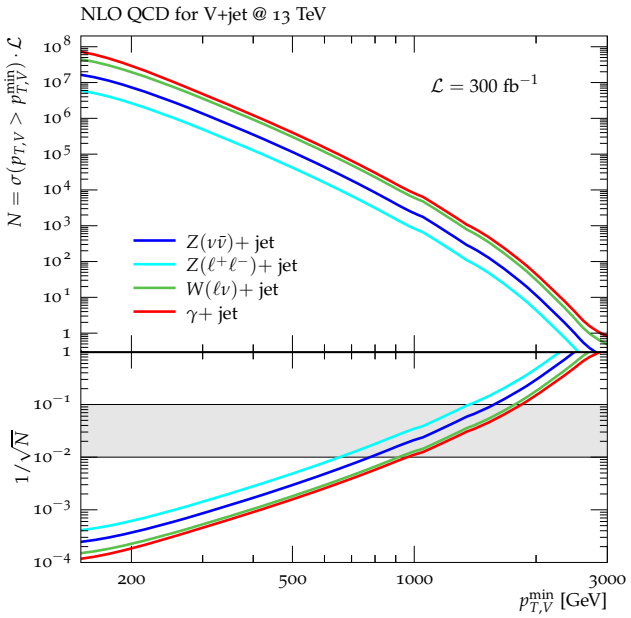

Figure 1: Production rates for $V+$jet(s), for various decay channels, as a function of the minimum $p_{\rm T}$ of the vector boson. Decays into $\ell^\pm = e^\pm, \mu^\pm$ and ν_e, ν_ν, ν_τ are included. The number of events, N, is normalized to $300\,{\rm fb}^{-1}$ of LHC data at $\sqrt{s} = 13\,{\rm TeV}$, and includes the basic selection cuts listed in the main body of the paper. The log lower panel shows the statistical uncertainties, calculated as $1/\sqrt{N}$. The gray band in the lower panel indicates the regime of 1–10% statistical uncertainty.

$Z(\nu\bar{\nu})+$jet production, followed by $W(\ell\nu)+$jet (in particular for $\ell = \tau$ or when the lepton is outside of the detector).[2] The experimental constraints on $Z(\nu\bar{\nu})+$jet production at large MET can be obtained from accurate measurements of $V+$jet production processes with visible vector-boson signatures. It is quite obvious, for example, that the measurement of $Z(\ell^+\ell^-)+$jets with $\ell = e, \mu$ is the most direct and reliable proxy for $Z(\nu\bar{\nu})+$jets. This control sample, however, is statistics limited, due to the smaller branching ratio of Z bosons to charged leptons relative to neutrinos. To extrapolate the shape of the Z spectrum to the largest $p_{\rm T}$ values, therefore, requires a theoretical prediction. The larger statistics of $W(\ell\nu)+$jets and $\gamma+$jets events makes it possible to directly access the relevant $p_{\rm T}$ range, but the relation between their spectra and the Z spectrum needs, once again, theoretical guidance.

To put things into a concrete perspective, Figure 1 shows the expected event rates, and the relative statistical uncertainty, for $300\,{\rm fb}^{-1}$ of integrated luminosity at 13 TeV. The extrapolation to the $\mathcal{O}(100\,{\rm fb}^{-1})$ and $\mathcal{O}(3000\,{\rm fb}^{-1})$ expected from the full run 2 and at the end of the full LHC programme, respectively, is straightforward. The $Z(\ell^+\ell^-)$+jets data allow for a direct estimate of the $Z(\nu\bar{\nu})$+jets rate with a statistical precision below 1% for $p_{\rm T}$ up to about 600 GeV. Using the $W(\ell\nu)$+jets or γ+jets data could in principle extend this range up to about 900 GeV. Beyond this value, the statistical precision of the $W(\ell\nu)$+jets and γ+jets events remains a factor of two better than that of the $Z(\nu\bar{\nu})$+jets signal. In order to ensure that the theoretical systematics in the extrapolation from the W+jets and γ+jets rates to the Z+jets rates remains negligible with respect to the statistical uncertainty, the former should be kept at the level of a few percent up to $p_{\rm T} \sim 2\,{\rm TeV}$, and around 10% up to $p_{\rm T} \sim 2.5 - 3\,{\rm TeV}$, which is the ultimate kinematic reach for the $Z(\nu\bar{\nu})$+jets signal at the end of LHC data taking.

[2]Other backgrounds (such as QCD multijets, $t\bar{t}$ or pairs of gauge bosons) are suppressed, and their contribution to the overall uncertainty is well below the percent level.

The main result of this work is to prove that, thanks to the recent theoretical advances, these goals can be met. This proof requires the analysis of a series of possible effects. On the one hand, the theoretical extrapolation to larger p_{T} of the very precise $Z(\ell^+\ell^-)$+jets data requires firm control over the shape of the distribution. Several effects, from the choice of parton distribution functions (PDFs) to the choices made for the renormalisation and factorisation scales used in the calculations, can influence the extrapolation. On the other hand, the level of correlation between the W, γ and Z spectra must be kept under control. At large p_{T}, in particular, large and process-dependent corrections arise due to the growth of the electroweak (EW) corrections, and these may spoil the correlation induced by pure QCD effects. For our analysis we shall use the most up-to-date theoretical predictions available today for the description of vector boson production at large p_{T}. On the QCD side, we rely on the next-to-next-to-leading order (NNLO) calculations, which appeared recently for Z+jet [8–12], W+jet [13, 14] and γ+jet [15, 16] production. On the EW side, we apply full NLO calculations for Z+jet [17–19], W+jet [19, 20] and γ+jet [21] production with off-shell decays of the Z and W bosons. Given the strong enhancement of EW Sudakov effects in the TeV region, we also include 2-loop logarithmic terms at next-to-leading logarithmic (NLL) accuracy for all $V+$ jet processes [23–26]. An extensive assessment and discussion of the estimates of missing higher-order terms, and of the relative systematics, is given in the main body of this paper. In particular, in order to address non-trivial issues that arise in the context of dark matter searches, we introduce a global framework for the estimate of theoretical uncertainties in all $V+$ jet processes, taking into account correlation effects across different processes and p_{T} regions. Also the uncertainties associated with the combination of QCD and EW corrections are discussed in detail.

From the experimental perspective, the determination of the background composition in signal and control regions, and the modeling of other key aspects of experimental analyses (e.g. lepton identification and reconstruction, missing energy, etc.) require a theoretical description of the various $V+$ jets processes at the particle level. Typically, this is provided by Monte Carlo (MC) samples based on multi-jet merging at LO or NLO QCD, and the reweighting of MC events is a standard approach that allows one to implement various possible improvements, such as higher-order QCD or EW corrections. For the fit of MC predictions to data, ATLAS and CMS analyses rely on the profile likelihood approach, where experimental and theoretical uncertainties are described in terms of nuisance parameters with Gaussian distributions. In this context, the correlations of theoretical uncertainties across p_{T} bins (shape uncertainties) and across different $V+$ jets processes play a key role for searches at large MET.

For the implementation of higher-order QCD and EW corrections and for the estimate of theoretical uncertainties in the experimental analysis framework, we propose a procedure based on a one-dimensional reweighting of MC samples. The proposed framework should enable the experiments to carry out their profile likelihood approach, quantifying the impact of the theoretical systematics in their analyses, and validating directly with data the reliability and robustness of the theoretical inputs. In this respect, we would like to stress that, independently of the application to BSM searches, the results in this paper provide a framework for incisive validations of the theoretical calculations. Furthermore, these results might allow for further constraints on PDFs [3, 27].

If the experimental analyses of the MET+jets channel should confirm the usefulness of the approach we propose, the same framework could be adapted to more complex or exclusive final states, in which for example MET is accompanied by a large number of (hard) jets or by specific objects (photons, heavy quarks, Higgs, etc). These extensions are left for future studies.

The structure of this paper is as follows: In Section 2 we introduce the reweighting technique, to incorporate in a MC analysis the effect of higher-order corrections and of

their systematic uncertainties including correlations. In Section 3 we discuss higher-order QCD and EW corrections, including the contribution of photon-initiated processes and real vector boson emission. We present here our approach to the estimate of the various systematics, covering QCD scale, shape and process-dependent uncertainties, as well as uncertainties arising from higher-order EW and mixed QCD–EW corrections. Section 4 describes details of the setup for numerical calculations presented in Section 3, the employed tools and methods, as well as the detailed definition of physics objects and observables to be used in the context of MC reweighting. Section 5 contains our summary and conclusions. As detailed in Appendix A, results for all V+jets processes are available in form of one-dimensional histograms in the vector-boson p_{T} covering central predictions and all mentioned uncertainties. Technical plots on the individual sources of QCD and EW uncertainties are documented in Appendix B.

2 Reweighting of Monte Carlo samples

The reweighting of MC samples is an approximate, but straightforward and easy to implement method of combining (N)LO MC simulations with (N)NLO QCD+NLO EW perturbative calculations and to account for the respective uncertainties in a systematic way. The following formula describes the one-dimensional reweighting of MC samples for $V+$jet production ($V = \gamma, Z, W^{\pm}$) in a generic variable x,

$$\frac{\mathrm{d}}{\mathrm{d}x}\frac{\mathrm{d}}{\mathrm{d}\vec{y}}\,\sigma^{(V)}(\vec{\varepsilon}_{\mathrm{MC}},\vec{\varepsilon}_{\mathrm{TH}}) = \frac{\mathrm{d}}{\mathrm{d}x}\frac{\mathrm{d}}{\mathrm{d}\vec{y}}\sigma^{(V)}_{\mathrm{MC}}(\vec{\varepsilon}_{\mathrm{MC}})\left[\frac{\frac{\mathrm{d}}{\mathrm{d}x}\sigma^{(V)}_{\mathrm{TH}}(\vec{\varepsilon}_{\mathrm{TH}})}{\frac{\mathrm{d}}{\mathrm{d}x}\sigma^{(V)}_{\mathrm{MC}}(\vec{\varepsilon}_{\mathrm{MC}})}\right]. \tag{1}$$

In the case at hand, i.e. $V+$jet production, the one-dimensional parameter x should be understood as the vector-boson transverse momentum, $x = p_{\mathrm{T}}^{(V)}$, while $\vec{y}$ generically denotes the remaining variables of the fully differential kinematic dependence of the accompanying QCD and QED activity, including both extra jet and photon radiation, as well as leptons and neutrinos from hadron decays. It is implicitly understood that $\frac{\mathrm{d}}{\mathrm{d}x}\frac{\mathrm{d}}{\mathrm{d}\vec{y}}\sigma$ depends on x and $\vec{y}$, while in $\frac{\mathrm{d}}{\mathrm{d}x}\sigma$ the variables $\vec{y}$ are integrated out.

The labels MC and TH in Eq. (1) refer to Monte Carlo and higher-order theoretical predictions, respectively, and the related uncertainties are parametrised through nuisance parameters $\vec{\varepsilon}_{\mathrm{TH}}, \vec{\varepsilon}_{\mathrm{MC}}$. Our recommendations for theory uncertainties in Section 3 are formulated in terms of intervals for the related nuisance parameters,

$$-1 < \varepsilon_{\mathrm{TH},k} < 1, \tag{2}$$

which pragmatically should be understood as the 1σ range of Gaussian uncertainties.

Monte Carlo uncertainties, described by $\vec{\varepsilon}_{\mathrm{MC}}$, must be correlated in the numerator and denominator on the r.h.s. of Eq. (1), while they can be kept uncorrelated across different processes (apart from $Z(\nu\bar{\nu})+$ jet and $Z(\ell^+\ell^-)+$ jet).

We note that, as opposed to an approach based only on ratios of p_{T} distributions, where theory is used for extrapolations across different processes at fixed p_{T}, MC reweighting is more powerful as it supports all possible extrapolations across different processes and p_{T} regions. In particular, it makes it possible to exploit $V+$jet precision measurements at moderate p_{T} in order to constrain $Z(\nu\bar{\nu})+$jet production in the TeV region.

A further advantage of the reweighting approach (1) lies in the fact that the three terms on the r.h.s. of Eq. (1) do not need to be computed with the same numerical setup (parameters, cuts, observables, etc.). More precisely, only the definition of the variable x and the binning of its distribution need to be the same in all three terms. Scale choices, QCD and EW input parameters and PDFs should be the same only in the numerator and

denominator of

$$R_{\rm MC}(x,\vec{y}) = \frac{\frac{\rm d}{{\rm d}x}\frac{\rm d}{{\rm d}\vec{y}}\sigma^{(V)}_{\rm MC}}{\frac{\rm d}{{\rm d}x}\sigma^{(V)}_{\rm MC}}, \tag{3}$$

but can be chosen in a different way in $\sigma^{(V)}_{\rm TH}$, provided that QCD and EW corrections themselves are computed using the same settings. Vice versa, possible cuts must be identical only in the numerator and denominator of

$$R_{\rm TH/MC}(x) = \frac{\frac{\rm d}{{\rm d}x}\sigma^{(V)}_{\rm TH}}{\frac{\rm d}{{\rm d}x}\sigma^{(V)}_{\rm MC}}, \tag{4}$$

while particle-level MC predictions, $\frac{\rm d}{{\rm d}x}\frac{\rm d}{{\rm d}\vec{y}}\sigma^{(V)}_{\rm MC}$, can be subject to more exclusive or inclusive cuts in the experimental analysis.

For an optimal combination of higher-order calculations and MC predictions, two conditions should be fulfilled. On the one hand, theory calculations should describe the distribution in the reweighting variable with higher (or at least equal) precision as compared to the MC sample,

$$\Delta\left[\frac{\rm d}{{\rm d}x}\sigma^{(V)}_{\rm TH}\right] \leq \Delta\left[\frac{\rm d}{{\rm d}x}\sigma^{(V)}_{\rm MC}\right]. \tag{5}$$

On the other hand, the MC sample should be more accurate than TH calculations in describing the correlation between x and all other variables $\vec{y}$,

$$\Delta\left[\frac{\frac{\rm d}{{\rm d}x}\frac{\rm d}{{\rm d}\vec{y}}\sigma^{(V)}_{\rm MC}}{\frac{\rm d}{{\rm d}x}\sigma^{(V)}_{\rm MC}}\right] \leq \Delta\left[\frac{\frac{\rm d}{{\rm d}x}\frac{\rm d}{{\rm d}\vec{y}}\sigma^{(V)}_{\rm TH}}{\frac{\rm d}{{\rm d}x}\sigma^{(V)}_{\rm TH}}\right]. \tag{6}$$

More precisely, condition (6) needs to be fulfilled only for those aspects of $V+$jet events that are relevant for the actual experimental analysis.

As concerns the first condition, we note that, depending on the choice of the observable x, using state-of-the-art theory calculations that involve higher-order QCD and EW corrections may not guarantee that Eq. (5) is fulfilled. In fact, there are a number of aspects, i.e. resolved multi-jet emissions, the resummation of soft logarithms in the region of small vector-boson $p_{\rm T}$, soft QCD radiation of non-perturbative origin, multiple photon radiation, or neutrinos and charged leptons resulting from hadron decays, for which fixed-order perturbative calculations are less accurate than MC simulations.

Thus, the reweighting variable x should be defined such as to have minimal sensitivity to the above-mentioned aspects. In this respect, due to its reduced sensitivity to multiple jet emissions, the vector-boson $p_{\rm T}$ is a natural choice. However, in order to fulfil Eq. (5), the region $p^{(V)}_{\rm T} \ll M_V$ should be excluded from the reweighting procedure, unless QCD Sudakov logarithms are resummed to all orders in the theoretical calculations. Moreover, in order to simultaneously fulfil conditions (5) and (6), any aspect of the reconstructed vector-boson $p_{\rm T}$ that is better described at MC level should be excluded from the definition of x and included in $\vec{y}$. This applies, as discussed in Section 4, to multiple photon emissions off leptons, and to possible isolation prescriptions for the soft QCD radiation that surrounds leptons or photons. In general, purely non-perturbative aspects of MC simulations, i.e. MPI, UE, hadronisation and hadron decays, should be systematically excluded from the definition of the reweighting variable x. Thus, impact and uncertainties related to this non-perturbative modelling will remain as in the original MC samples.

It should be stressed that the above considerations are meant for dark-matter searches based on the *inclusive* MET distribution, while more exclusive searches that exploit additional information on hard jets may involve additional subtleties. In particular, for analyses that are sensitive to multi-jet emissions, using the inclusive vector-boson $p_{\rm T}$ as

the reweighting variable would still fulfil Eq. (5), but the lack of QCD and EW corrections to $V + 2\,\text{jets}$ production in MC simulations could lead to a violation of Eq. (6). In analyses that are sensitive to the tails of inclusive jet-p_{T} and H_{T} distributions this issue is very serious, and QCD+EW corrections should be directly implemented at MC level using multi-jet merging [19].

In general, as a sanity check of the reweighting procedure, we recommend verifying that, for reasonable choices of input parameters and QCD scales, (N)NLO QCD calculations and (N)LO merged MC predictions for vector-boson p_{T} distributions are in reasonably good agreement within the respective uncertainties. Otherwise, in case of significant MC mismodelling of the $\frac{\text{d}}{\text{d}x}\sigma^{(V)}$ distribution, one should check the reliability of the MC in extrapolating TH predictions from the reweighting distribution to other relevant observables.

In general, one could check whether the one-dimensional reweighting via the variable x in Eq. (1) can in fact reproduce the dependence of the corrections in other kinematic variables that are relevant for the experimental analysis. To this end, distributions of $\sigma^{(V)}$ w.r.t. another kinematic variable x' should be calculated upon integrating Eq. (1). Switching on and off the corrections on the r.h.s. of Eq. (1) in $\sigma^{(V)}_{\text{TH}}$ and taking the ratio of the obtained differential cross sections $\sigma^{(V)}$, produces the relative correction to the x' distribution that could be directly compared to the corresponding result directly calculated from $\sigma^{(V)}_{\text{TH}}$.[3]

Finally, it is crucial to check that state-of-the-art predictions for absolute $\text{d}\sigma/\text{d}p_{\text{T}}$ distributions agree with data for the various visible final states.

3 Higher-order QCD and EW predictions

Precise theory predictions for $V+\text{jet}$ production require QCD and EW higher-order corrections, mixed QCD–EW contributions, as well as photon-induced contributions,

$$\frac{\text{d}}{\text{d}x}\sigma^{(V)}_{\text{TH}} = \frac{\text{d}}{\text{d}x}\sigma^{(V)}_{\text{QCD}} + \frac{\text{d}}{\text{d}x}\Delta\sigma^{(V)}_{\text{EW}} + \frac{\text{d}}{\text{d}x}\Delta\sigma^{(V)}_{\text{mix}} + \frac{\text{d}}{\text{d}x}\sigma^{(V)}_{\gamma-\text{ind.}}. \tag{7}$$

State-of-the art QCD and EW predictions and the related theoretical uncertainties are discussed in Sections 3.1–3.2. Section 3.3 is devoted to photon-induced channels and PDF uncertainties. In Section 3.4 we discuss the real emission of vector bosons. Mixed corrections of $\mathcal{O}(\alpha\alpha_{\text{S}})$ are addressed in Section 3.5 by means of a factorised combination of QCD and EW corrections.

Besides the general theoretical framework, in this section we present various plots that illustrate the effect of higher-order corrections and uncertainties for $pp \to V+\text{jet}$ at a centre-of-mass energy of 13 TeV. The input parameters, as well as the relevant selection criteria for observables involving leptons and photons, are specified in Section 4. As is well known, photon isolation plays a critical role for the behaviour of QCD corrections in $\gamma+\text{jet}$ production and for the correlation of QCD uncertainties between $\gamma+\text{jet}$ and $Z/W+\text{jet}$ production. The issue of photon isolation is discussed in detail in Section 4.1, where we propose a dynamic cone isolation prescription that renders the QCD dynamics of $pp \to \gamma+\text{jet}$ and $pp \to Z/W+\text{jet}$ very similar at large transverse momenta. This feature provides a very convenient basis for a systematic modelling of the correlation of QCD uncertainties between the various $V+\text{jet}$ production processes as discussed in Section 3.1 and 4.1. In Section 4.4 we detail the tools that have been employed for obtaining the predictions presented in this work.

For the sake of a complete documentation, we provide data sets (see Appendix A) for vector-boson p_{T} spectra above 30 GeV, while we plot results starting at 80 GeV. We note

[3] This procedure should be restricted to variables x' that can be described with decent accuracy both in perturbative calculations and in the MC simulations.

that in the region of $p_{\rm T} \lesssim 100$ GeV there are potential sources of systematics that we are not controlling or even discussing, as they would require a separate study. These arise from the resummation of QCD Sudakov logarithms or from non-perturbative effects (e.g. an order $\Lambda_{\rm QCD}$ average shift of the vector boson $p_{\rm T}$ associated with the asymmetry of colour flow in the final state). Furthermore, as shown later, a reliable correlation between the Z/W spectra and the photon spectrum requires $p_{\rm T}$ to be large enough so that fragmentation contributions in γ+jet production become small. We also expect that in the $p_{\rm T}$ regions up to a few hundred GeV the statistics are sufficient to guarantee that experimental analyses of missing-$E_{\rm T}$ backgrounds can entirely rely on the direct measurement of the Z spectrum measured via $Z \to \ell^+\ell^-$. As a result, we believe that our conclusions on the systematic uncertainties are most reliable and useful for experimental applications in the region of $p_{\rm T}$ larger than 100–200 GeV.

3.1 Higher-order QCD predictions

For perturbative QCD predictions at LO, NLO and NNLO we use the generic notation

$$\frac{\mathrm{d}}{\mathrm{d}x}\sigma^{(V)}_{\rm QCD} = \frac{\mathrm{d}}{\mathrm{d}x}\sigma^{(V)}_{\rm N^kLO\,QCD}, \tag{8}$$

with $k = 0, 1$ or 2. Wherever possible, nominal predictions are provided at NNLO QCD, i.e. including terms up to[4] $\mathcal{O}(\alpha\alpha_{\rm S}^3)$. However, as ingredients for the assessment of some theory uncertainties, also LO and NLO QCD contributions will be used.

For convenience, results at N^{k}LO QCD are systematically expressed in terms of LO predictions and relative correction factors defined through

$$\frac{\mathrm{d}}{\mathrm{d}x}\sigma^{(V)}_{\rm N^kLO\,QCD}(\vec{\mu}) \;=\; K^{(V)}_{\rm N^kLO}(x,\vec{\mu})\frac{\mathrm{d}}{\mathrm{d}x}\sigma^{(V)}_{\rm LO\,QCD}(\vec{\mu}_0). \tag{9}$$

We calculate all N^{k}LO and LO cross sections with one and the same set of NNLO PDFs as discussed in Section 4.3. The dependence on the renormalisation and factorisation scales, $\vec{\mu} = (\mu_R, \mu_F)$, is absorbed into the K-factors, while LO predictions on the r.h.s. of Eq. (9) are taken at the central scale, $\vec{\mu}_0 = (\mu_{R,0}, \mu_{F,0})$. For the central scale we adopt the commonly used choice

$$\mu_{R,0} = \mu_{F,0} = \mu_0 = \hat{H}'_{\rm T}/2, \tag{10}$$

where the total transverse energy, $\hat{H}'_{\rm T}$, is defined as the scalar sum of the transverse energy of all parton-level final-state objects,

$$\hat{H}'_{\rm T} = E_{{\rm T},V} + \sum_{i\in\{\rm q,g,\gamma\}} |p_{{\rm T},i}|. \tag{11}$$

Also quarks (q), gluons (g) and photons that are radiated at (N)NLO are included in $\hat{H}'_{\rm T}$, and the vector-boson transverse energy, $E_{{\rm T},V}$, is computed using the total (off-shell) four-momentum of the corresponding decay products, i.e.

$$E^2_{\rm T,Z} = p^2_{{\rm T},\ell^+\ell^-} + m^2_{\ell^+\ell^-}, \qquad E^2_{\rm T,W} = p^2_{{\rm T},\ell\nu} + m^2_{\ell\nu}, \qquad E^2_{{\rm T},\gamma} = p^2_{{\rm T},\gamma}. \tag{12}$$

In order to guarantee infrared safety at NLO EW, the scale (11) must be insensitive to collinear photon emissions off charged fermions. To this end, the vector-boson transverse energies defined in Eq. (12) should be computed in terms of dressed leptons as specified in Section 4.1, while $|p_{{\rm T},\gamma}|$ contributions to Eq. (11) should involve only photons that have not been recombined with charged leptons. It is worth to note that $\mu_0 \approx p_{{\rm T},V}$ at large $p_{{\rm T},V}$.

[4] Here and in the following we adopt a power counting that does not include the extra factor α associated with vector-boson decays.

Pure QCD uncertainties

The uncertainty associated with the truncation of the perturbative expansion in α_S is estimated by means of factorisation and renormalisation scale variations. On the one hand, we consider standard seven-point variations applying, respectively, factor-two rescalings, i.e.

$$\frac{\vec{\mu}_i^{(1)}}{\mu_0} = (1,1),(2,2),(0.5,0.5),(2,1),(1,2),(1,0.5),(0.5,1), \tag{13}$$

where $i = 0,\ldots 6$. Nominal predictions and related uncertainties are defined as the centre and the half-width of the band resulting from the above variations. In terms of K-factors this corresponds to

$$K^{(V)}_{\mathrm{N}^k\mathrm{LO}}(x) = \frac{1}{2}\left[K^{(V,\max)}_{\mathrm{N}^k\mathrm{LO}}(x) + K^{(V,\min)}_{\mathrm{N}^k\mathrm{LO}}(x)\right], \tag{14}$$

$$\delta^{(1)}K^{(V)}_{\mathrm{N}^k\mathrm{LO}}(x) = \frac{1}{2}\left[K^{(V,\max)}_{\mathrm{N}^k\mathrm{LO}}(x) - K^{(V,\min)}_{\mathrm{N}^k\mathrm{LO}}(x)\right], \tag{15}$$

with

$$\begin{aligned} K^{(V,\max)}_{\mathrm{N}^k\mathrm{LO}}(x) &= \max\left\{K^{(V)}_{\mathrm{N}^k\mathrm{LO}}(x,\vec{\mu}_i^{(k)})\,|0\le i\le 6\right\},\\ K^{(V,\min)}_{\mathrm{N}^k\mathrm{LO}}(x) &= \min\left\{K^{(V)}_{\mathrm{N}^k\mathrm{LO}}(x,\vec{\mu}_i^{(k)})\,|0\le i\le 6\right\}. \end{aligned} \tag{16}$$

Since the shift resulting form the symmetrisation of scale variations in Eq. (14) is encoded in the K-factors, also the LO K-factor differs from one.

Constant scale variations mainly affect the overall normalisation of p_{T}-distributions and tend to underestimate shape uncertainties, which play an important role in the extrapolation of low-p_{T} measurements to high p_{T}. Thus, for a reasonably conservative estimate of shape uncertainties, we introduce an additional variation,

$$\delta^{(2)}K^{(V)}_{\mathrm{N}^k\mathrm{LO}}(x) = \omega_{\mathrm{shape}}(x)\,\delta^{(1)}K^{(V)}_{\mathrm{N}^k\mathrm{LO}}(x), \tag{17}$$

where the standard scale uncertainty (15) is supplemented by a shape distortion $\omega_{\mathrm{shape}}(x)$, with $|\omega_{\mathrm{shape}}(x)| \le 1$ and $\omega_{\mathrm{shape}}(x) \to \pm 1$ at high and small transverse momentum, respectively. The function ω_{shape} is defined as

$$\omega_{\mathrm{shape}}(p_{\mathrm{T}}) = \tanh\left[\ln\left(\frac{p_{\mathrm{T}}}{p_{\mathrm{T},0}}\right)\right] = \frac{p_{\mathrm{T}}^2 - p_{\mathrm{T},0}^2}{p_{\mathrm{T}}^2 + p_{\mathrm{T},0}^2}, \tag{18}$$

and as reference transverse momentum we choose the value $p_{\mathrm{T},0} = 650\,\mathrm{GeV}$, which corresponds (in logarithmic scale) to the middle of the range of interest, 0.2–2 TeV. As illustrated in Figure 2, the function $\omega_{\mathrm{shape}}(x)$ induces asymmetric variations that cover $\pm 75\%$ of the standard scale variation band for $p_{\mathrm{T}} \in [250, 1750]\,\mathrm{GeV}$. Note that, in the combination of the uncertainties (15) and (17), our choice to have an additional shape variation augments the standard scale uncertainty by a factor $1 \le \sqrt{1+\omega^2_{\mathrm{shape}}(p_{\mathrm{T}})} \le \sqrt{2}$.

From the viewpoint of QCD interactions, the various $V+$jet production processes are quite similar to each other at $p_{\mathrm{T},V} \gg M_{W,Z}$. However, due to the presence of $q \to q\gamma$ collinear singularities and the need to suppress them with an appropriate photon-isolation prescription, QCD corrections in $\gamma+$jet production can feature significant differences as compared to the case of $pp \to W/Z+$jet. In Section 4.1 we introduce a dynamic photon isolation prescription that renders the QCD dynamics of $pp \to \gamma+$jet and $pp \to Z/W+$jet processes almost universal, i.e independent of the nature of the produced vector bosons.

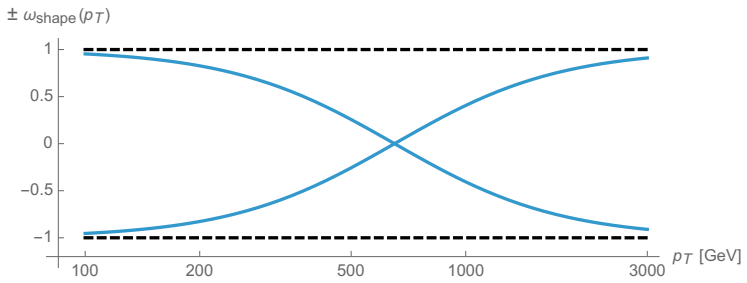

Figure 2: Shape variation function $\omega_{\rm shape}(p_{\rm T})$ defined in Eq. (18).

With this dynamic photon isolation, which is used as default in this study, QCD K-factors and related uncertainties are very strongly correlated across all $V+$jet processes, i.e. $K^{(V)}_{{\rm N}^k{\rm LO}}(x)$ and $\delta^{(i)}K^{(V)}_{{\rm N}^k{\rm LO}}(x)$ depend only very weakly on V at high $p_{\rm T}$.[5]

The correlation of QCD uncertainties across $V+$jet processes plays a key role in fits of the $Z(\nu\bar{\nu})+$jet dark matter background, and the quantitative understanding of such process correlations belongs to the most important theoretical aspects in dark matter searches. To this end we introduce a specific uncertainty based on the process dependence of the highest available term in the perturbative expansion,

$$\Delta K^{(V)}_{{\rm N}^k{\rm LO}}(x) = K^{(V)}_{{\rm N}^k{\rm LO}}(x)/K^{(V)}_{{\rm N}^{k-1}{\rm LO}}(x) - 1. \tag{19}$$

Specifically, as a conservative estimate of unknown process correlation effects, we take the difference of the known QCD K-factors with respect to $Z+$jet production,

$$\delta^{(3)}K^{(V)}_{{\rm N}^k{\rm LO}}(x) \;=\; \Delta K^{(V)}_{{\rm N}^k{\rm LO}}(x) - \Delta K^{(Z)}_{{\rm N}^k{\rm LO}}(x). \tag{20}$$

The process correlation uncertainty (20) can be assessed using the central scale (10) throughout. While the choice of $Z+$jet production as reference process is arbitrary, changing the reference process has very little impact on process correlations since the resulting overall shift in $\delta^{(3)}K^{(V)}_{{\rm N}^k{\rm LO}}(x)$ cancels to a large extent in ratios of $V+$jet cross sections. Note that, since the $V+$jet K-factors of the same order k are strongly correlated, the small process-dependent parts of K-factors, $\delta^{(3)}K^{(V)}_{{\rm N}^k{\rm LO}}(x) \ll \Delta K^{(V)}_{{\rm N}^k{\rm LO}}$, are downgraded from the status of known higher-order corrections to uncertainties without excessive losses of accuracy in the nominal N^{k}LO predictions for individual processes.

This modelling of process correlations assumes a close similarity of QCD effects between all $pp \to V+$jet processes. This is achieved by means of the dynamic photon isolation prescription of Section 4.1, while the fact that experimental analyses employ a quite different photon isolation approach requires an additional $\gamma+$jet specific uncertainty discussed in Section 4.1.

The above uncertainties can be parametrised through a set of independent nuisance parameters, $\vec{\varepsilon}_{\rm QCD}$, and combined using

$$\begin{aligned}\frac{{\rm d}}{{\rm d}x}\sigma^{(V)}_{{\rm N}^k{\rm LO}\,{\rm QCD}}(\vec{\varepsilon}_{\rm QCD}) \;&=\; \left[K^{(V)}_{{\rm N}^k{\rm LO}}(x) + \sum_{i=1}^{3}\varepsilon_{{\rm QCD},i}\,\delta^{(i)}K^{(V)}_{{\rm N}^k{\rm LO}}(x)\right] \\ &\quad\times \frac{{\rm d}}{{\rm d}x}\sigma^{(V)}_{{\rm LO}\,{\rm QCD}}(\vec{\mu}_0).\end{aligned} \tag{21}$$

The nuisance parameters $\varepsilon_{{\rm QCD},1}, \varepsilon_{{\rm QCD},2}$ and $\varepsilon_{{\rm QCD},3}$ should be Gaussian distributed with one standard deviation corresponding to the range $\varepsilon_{{\rm QCD},i} \in [-1,+1]$. These parameters

[5] For what concerns process correlations, it is crucial that (apart from the M_V dependence) all $V+$jet processes are evaluated using equivalent dynamical scales.

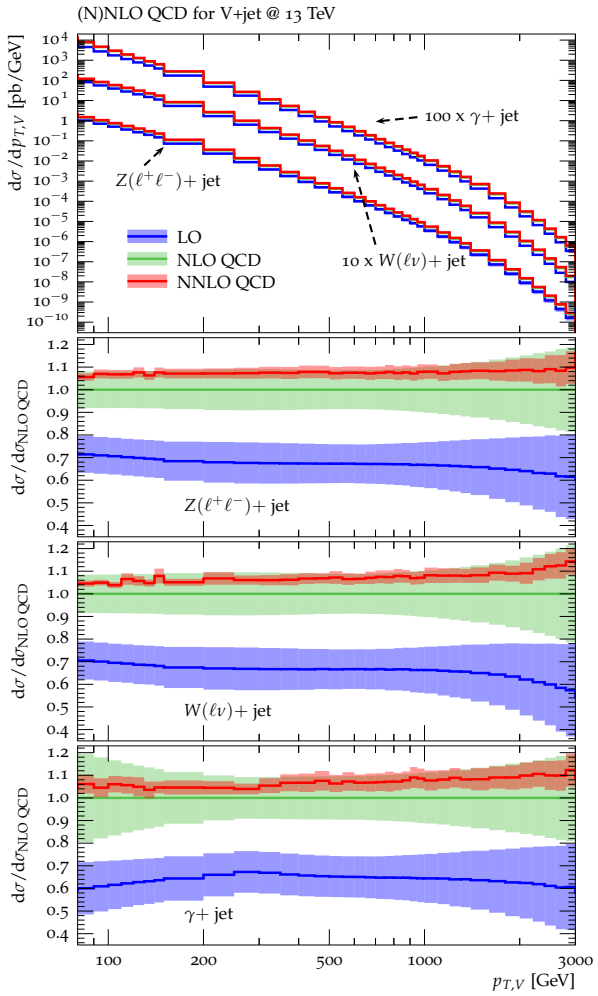

Figure 3: Higher-order QCD predictions and uncertainties for $Z(\ell^+\ell^-)$+jet, $W^\pm(\ell\nu)$+jet, and γ+jet production at 13 TeV. Absolute predictions at LO, NLO and NNLO QCD are displayed in the main frame. In the ratio plots all results are normalised to NLO QCD, and the bands at LO and NLO correspond to the combination (in quadrature) of the three types of QCD uncertainties, $\delta^{(i)}K_{\mathrm{N}^k\mathrm{LO}}$, i.e. scale uncertainties according to Eq. (15), shape uncertainties according to Eq. (17), and process-correlation uncertainties according to Eq. (20). The band at NNLO corresponds to just scale uncertainties.

should be kept uncorrelated, but each $\varepsilon_{\mathrm{QCD},i}$-variation should be applied in a correlated way across p_{T} bins and processes, since correlation effects are consistently implemented in the $\delta^{(i)}K^{(V)}_{\mathrm{N}^k\mathrm{LO}}(x)$ terms.

Numerical results

In Figures 3–5 we show the effect of highers-order QCD corrections on the different V+jets processes together with the corresponding uncertainty estimates $\delta^{(i)}K_{\mathrm{N}^k\mathrm{LO}}$. See also Figure 18 in Appendix B. In Figure 3 the three uncertainty contributions are combined (in quadrature) while in Figure 5 (and in Figure 18) they are shown separately. Ratios of p_{T}-distributions for different processes are shown in Figure 4. See also Figure 19 in Appendix B. In Figure 4 again the different QCD uncertainties are combined in quadrature. The NLO corrections and uncertainties to Z+jet and W+jet production are almost identical over large p_{T} regions, where here and in the following W denotes W^+ and W^-

combined.

They amount to 25–30% with respect to LO. Only at very large p_{T} the NLO corrections to W+jet grow faster than in the case of Z+jet. This results in an increase of the process correlation uncertainty $\delta^{(3)}K_{\mathrm{NLO}}$ up to about 5% beyond $p_{\mathrm{T}} = 2$ TeV. For lower p_{T}, the NLO corrections to the two processes agree at the level of 1–2%. Scale uncertainties $\delta^{(1)}K_{\mathrm{NLO}}$ and shape uncertainties $\delta^{(2)}K_{\mathrm{NLO}}$ amount to 10–15% and are almost identical for the two processes. Thus they largely cancel in the Z/W ratio. A similar amount of agreement of the higher-order QCD dynamics can be observed comparing the high-p_{T} behaviour of Z+jet and γ+jet production. This is a consequence of the dynamical cone isolation in γ+jet, as discussed above. However, below $p_{\mathrm{T}} \approx 200$ GeV, mass effects render the two processes fundamentally different yielding sizeable process correlation uncertainties in γ+jet. At higher p_{T}, scale and shape uncertainties almost exactly cancel in the Z/γ ratio, and the total QCD uncertainty is dominated by the process correlation uncertainty. At $p_{\mathrm{T}} \approx 300$ GeV the process correlation uncertainty in γ+jet becomes accidentally very small (see Figure 18) yielding a pinch in the total QCD uncertainty in the Z/γ and the W/γ ratios. However, one should keep in mind that an additional analysis-dependent photon-isolation uncertainty, see Section 4.1, has to be considered for these ratios. The NNLO corrections to the nominal p_{T}-distributions amount to about 5–10% with respect to NLO and reduce the scale uncertainties at the level of 2–5%. The NNLO corrections behave very similarly across the different processes, confirming the universality of QCD dynamics in V+jet production. In fact, as shown in Figure 4, the process ratios are remarkably stable going from LO via NLO to NNLO. The predictions of the process ratios at NNLO confirm the percent-level uncertainties anticipated at NLO.

3.2 Electroweak corrections

For EW higher-order corrections we use the notation,

$$\begin{aligned} \frac{\mathrm{d}}{\mathrm{d}x}\sigma^{(V)}_{\mathrm{NLO\,EW}} &= \frac{\mathrm{d}}{\mathrm{d}x}\sigma^{(V)}_{\mathrm{LO\,QCD}} + \frac{\mathrm{d}}{\mathrm{d}x}\Delta\sigma^{(V)}_{\mathrm{NLO\,EW}}, \\ \frac{\mathrm{d}}{\mathrm{d}x}\sigma^{(V)}_{\mathrm{nNLO\,EW}} &= \frac{\mathrm{d}}{\mathrm{d}x}\sigma^{(V)}_{\mathrm{NLO\,EW}} + \frac{\mathrm{d}}{\mathrm{d}x}\Delta\sigma^{(V)}_{\mathrm{NNLO\,Sud}}, \end{aligned} \tag{22}$$

where $\Delta\sigma^{(V)}_{\mathrm{NLO\,EW}}$ denotes exact $\mathcal{O}(\alpha^2\alpha_{\mathrm{S}})$ contributions, and NNLO Sud stands for $\mathcal{O}(\alpha^3\alpha_{\mathrm{S}})$ EW Sudakov logarithms in NLL approximation (see below). Their combination is dubbed nNLO EW as it accounts for the dominant EW effects at NNLO. While our power counting does not consider the extra factor α associated with vector-boson decays, all predictions for $pp \to W/Z+$jet at (N)NLO QCD + NLO EW are at the level of the full processes, $pp \to \ell\nu/\ell\ell/\nu\nu+$jet, including off-shell effects and NLO EW corrections in decays. Since EW Sudakov logarithms do not enter W and Z decays, they are applied only at the level of $pp \to V+$jet production, including off-shell decays at LO.

The EW corrections, similarly as for the QCD ones, are also expressed in terms of correction factors with respect to LO QCD,

$$\frac{\mathrm{d}}{\mathrm{d}x}\sigma^{(V)}_{\mathrm{EW}}(\vec{\mu}) = \left[1 + \kappa^{(V)}_{\mathrm{EW}}(x,\vec{\mu})\right]\frac{\mathrm{d}}{\mathrm{d}x}\sigma^{(V)}_{\mathrm{LO\,QCD}}(\vec{\mu}), \tag{23}$$

where EW stands for NLO EW or nNLO EW. At variance with Eq. (9), here the EW κ-factors are defined by taking the factorized LO cross section at the same QCD scales, $\vec{\mu} = (\mu_{\mathrm{R}}, \mu_{\mathrm{F}})$, as in the higher-order EW prediction. In this way, since QCD scale variations at LO QCD and (n)NLO EW have almost identical impact, the relative EW correction is essentially independent of $\vec{\mu}$. Thus, in practice, κ_{EW} can be computed at the fixed reference scale,

$$\kappa^{(V)}_{\mathrm{EW}}(x,\vec{\mu}) \simeq \kappa^{(V)}_{\mathrm{EW}}(x,\vec{\mu}_0) = \kappa^{(V)}_{\mathrm{EW}}(x), \tag{24}$$

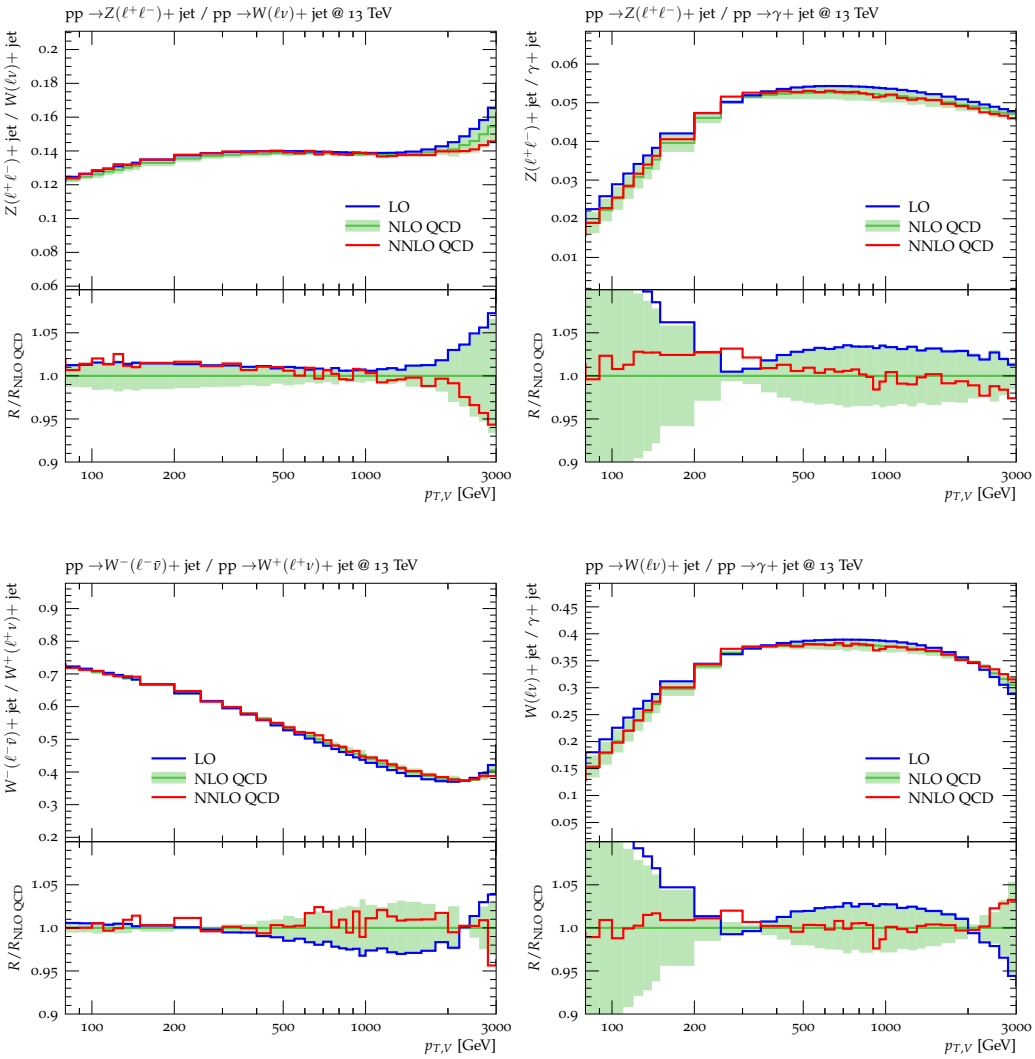

Figure 4: Ratios of p_{T}-distributions for various $pp \to V+$jet processes at LO, NLO QCD and NNLO QCD. The NLO QCD uncertainties, estimated according to Eq. (15), Eq. (17), and Eq. (20) are correlated amongst all processes and combined in quadrature. At LO and NNLO only nominal predictions are shown.

while the scale dependence of $\sigma^{(V)}_{\mathrm{EW}}$ is generated through $\sigma^{(V)}_{\mathrm{LO\,QCD}}(\vec{\mu})$ in Eq. (23). Moreover, the EW correction factor $\kappa^{(V)}_{\mathrm{EW}}$ is rather insensitive to the choice of PDF set as long as it is derived from cross sections that are based on the same PDFs. Analogously to Eq. (22), nNLO EW correction factors are split into a full NLO part and an NNLO Sudakov part,

$$\kappa^{(V)}_{\mathrm{nNLO\,EW}}(x) = \kappa^{(V)}_{\mathrm{NLO\,EW}}(x) + \kappa^{(V)}_{\mathrm{NNLO\,Sud}}(x). \tag{25}$$

At NLO EW, all relevant contributions of $\mathcal{O}(\alpha^2\alpha_{\mathrm{S}})$ are included. In the $q\bar{q}$ channel, and in all crossing-related channels, they comprise the following types of corrections:

(a.1) virtual EW corrections to $q\bar{q} \to Vg$;

(a.2) $q\bar{q} \to Vg\gamma$ photon bremsstrahlung;

(a.3) virtual QCD corrections to $q\bar{q} \to V\gamma$, which are needed to cancel soft-gluon singularities from (a.2) if the final-state QCD partons are allowed to become unresolved;

(a.4) $q\bar{q} \to Vq'\bar{q}'$ bremsstrahlung, which contributes at $\mathcal{O}(\alpha^2\alpha_{\mathrm{S}})$ through the interference of $\mathcal{O}(eg_S^2)$ and $\mathcal{O}(e^3)$ tree amplitudes in the same-flavour case, $q = q'$;

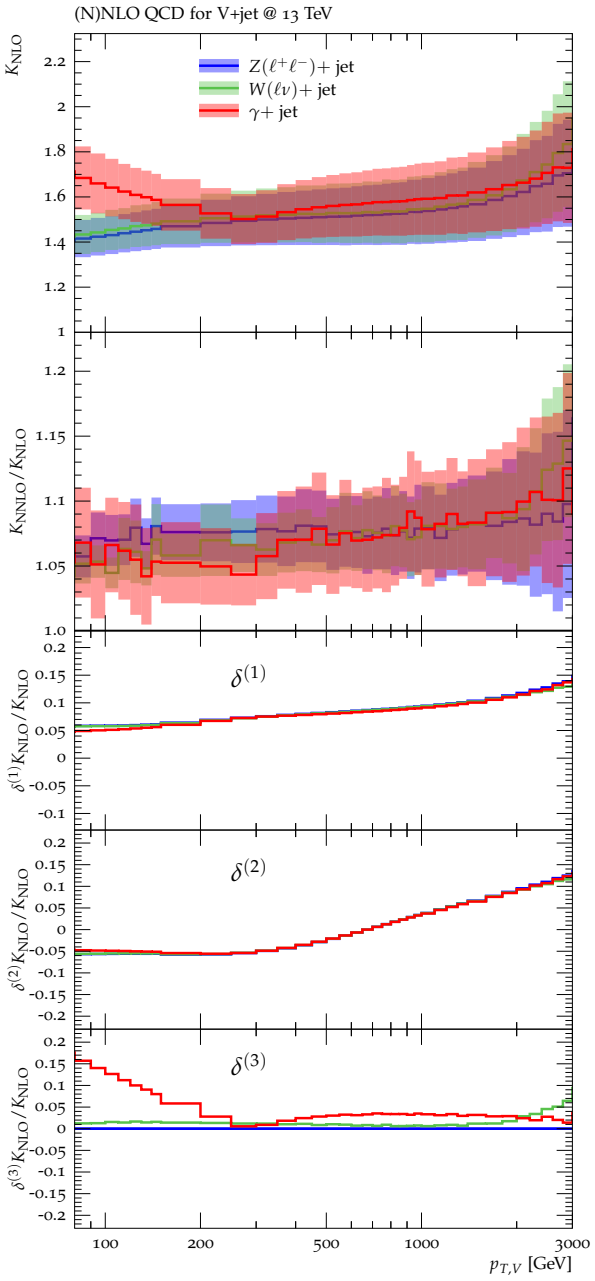

Figure 5: QCD K-factors at NLO (with respect to LO) and NNLO (with respect to NLO) for the various $pp \to V+\text{jet}$ processes at 13 TeV. The bands in the two upper frames correspond to scale variations, i.e. $\delta^{(1)}K_{\rm NLO}$ and $\delta^{(1)}K_{\rm NNLO}$. The lower frames show the individual uncertainties defined in Eq. (15), Eq. (17), and Eq. (20) at NLO. They are displayed as ratios $\delta^{(i)}K_{\rm NLO}/K_{\rm NLO}$, which corresponds to the relative impact of uncertainties on $p_{\rm T}$ distributions at NLO.

Formally at this order in perturbation theory also the following contributions appear and are not included:

(a.5) $\gamma q \to Vqg$ photon-induced quark-bremsstrahlung[6], at $\mathcal{O}(\alpha^2\alpha_S)$, which plays the dual role of NLO EW correction to the $q\bar{q} \to Vg$ channel and NLO QCD correction to the $\gamma q \to Vq$ channel. As discussed in Section 3.3, given the relatively small impact of $\gamma q \to Vq$ processes at $\mathcal{O}(\alpha^2)$, photon-induced contributions of $\mathcal{O}(\alpha_S\alpha^2)$ will not be included in the present study;

(a.6) real-boson emission, i.e. $pp \to VV'j$, contributes at $\mathcal{O}(\alpha^2\alpha_S)$. However, as discussed in Section 3.4, in order to avoid double counting with diboson production, such contributions should be treated as separate background samples and not as part of the EW corrections to $pp \to Vj$.

At very high transverse momentum, EW corrections are strongly enhanced by Sudakov effects, and the inclusion of higher-order Sudakov logarithms becomes mandatory in order to achieve few-percent level accuracy. In the high-p_T regime, where all energy scales are far above the weak-boson mass scale, higher-order virtual EW corrections to hard scattering cross sections can be described by means of resummation formulas of the type[7] [28]

$$\mathrm{d}\sigma_{\mathrm{EW}} = \exp\left\{\int_{M_W^2}^{Q^2} \frac{\mathrm{d}t}{t}\left[\int_{M_W^2}^{t} \mathrm{d}\tau \frac{\gamma(\alpha(\tau))}{\tau} + \chi(\alpha(t)) + \xi\left(\alpha(M_W^2)\right)\right]\right\} \mathrm{d}\sigma_{\mathrm{hard}}, \tag{26}$$

where γ, χ and ξ are anomalous dimensions depending on the EW quantum numbers of the scattering particles. The hard cross section has the form

$$\mathrm{d}\sigma_{\mathrm{hard}} = \left[1 + \frac{\alpha}{\pi}\delta_{\mathrm{hard}}^{(1)} + \left(\frac{\alpha}{\pi}\right)^2 \delta_{\mathrm{hard}}^{(2)} + \dots\right] \mathrm{d}\sigma_{\mathrm{Born}}, \tag{27}$$

and the correction factors $\delta_{\mathrm{hard}}^{(k)}$ are finite in the limit $Q^2/M_W^2 \to \infty$, while EW Sudakov and subleading high-energy logarithms of type $\alpha^m \ln^n\left(Q^2/M_W^2\right)$ are factorised in the exponential. Expanding in $\alpha = \alpha(M^2)$ with $\gamma_i(\alpha) = \frac{\alpha}{\pi}\gamma_i^{(1)} + \dots$, and $\alpha(t) = \alpha\left[1 + \frac{\alpha}{\pi}b^{(1)}\ln\left(\frac{t}{M^2}\right) + \dots\right]$ yields

$$\exp\left\{\dots\right\} = 1 + \frac{\alpha}{\pi}\delta_{\mathrm{Sud}}^{(1)} + \left(\frac{\alpha}{\pi}\right)^2 \delta_{\mathrm{Sud}}^{(2)} + \dots. \tag{28}$$

At NLL level, which is the logarithmic accuracy at which NNLO Sudakov effects are known for $V+$jet production [22–26], the following types of logarithms are available,

$$\begin{aligned}
\delta_{\mathrm{Sud}}^{(1)} &= \sum_{i,j} C_{2,ij}^{(1)} \ln^2\left(\frac{Q_{ij}^2}{M^2}\right) + C_1^{(1)} \ln^1\left(\frac{Q^2}{M^2}\right), \\
\delta_{\mathrm{Sud}}^{(2)} &= \sum_{i,j} C_{4,ij}^{(2)} \ln^4\left(\frac{Q_{ij}^2}{M^2}\right) + C_3^{(2)} \ln^3\left(\frac{Q^2}{M^2}\right) + \mathcal{O}\left[\ln^2\left(\frac{Q^2}{M^2}\right)\right],
\end{aligned} \tag{29}$$

where $M = M_W \sim M_Z$, $Q_{ij}^2 = |(\hat{p}_i \pm \hat{p}_j)^2|$ are the various Mandelstam invariants built from the hard momenta $\hat{p}_i$ of the $V+$jet production process and $Q^2 = Q_{12}^2 = \hat{s}$.

[6] Note that, in spite of the fact that we present them as separate terms in Eq. (7), γ-induced contributions and NLO EW corrections to $pp \to V+$jet are interconnected at $\mathcal{O}(\alpha^2\alpha_S)$.

[7] Here, in order to discuss qualitative features of Sudakov logarithms, we adopt a generic and rather schematic representation of the asymptotic high-energy limit. In particular, we do not consider some aspects, such as the helicity dependence of the corrections or SU(2) soft-correlation effects. However, in the numerical analysis all relevant aspects are consistently included.

In this work we will employ the explicit NLL Sudakov results of Refs. [22–26], which have been implemented, in addition to exact NLO QCD+NLO EW amplitudes, in the OpenLoops matrix-element generator [19, 29]. Let us recall that the results of Refs. [22–26] are based on the high-energy limit of virtual one- and two-loop corrections regularised with a fictitious photon mass of order M_W. This generates logarithms of the form $\alpha^n \ln^k(\hat{s}/M_W^2)$ that correspond to the combination of virtual one- and two-loop EW corrections plus corresponding photon radiation contributions up to an effective cut-off scale of order M_W. In the case of $V+$jet production, for physical observables that are inclusive with respect to photon radiation, this approximation is accurate at the one-percent level [21, 23, 26].

In this work we will employ full EW results at NLO and NLL Sudakov logarithms at NNLO. In the notation of Eqs. (23)–(25), for fully-differential partonic cross sections, this implies

$$\kappa_{\text{NLO EW}}(\hat{s},\hat{t}) = \frac{\alpha}{\pi}\left[\delta^{(1)}_{\text{hard}} + \delta^{(1)}_{\text{Sud}}\right], \tag{30}$$

$$\kappa_{\text{NNLO Sud}}(\hat{s},\hat{t}) = \left(\frac{\alpha}{\pi}\right)^2 \delta^{(2)}_{\text{Sud}}. \tag{31}$$

Transverse-momentum distributions including exact NLO EW corrections and Sudakov logarithms at NLO and NNLO are shown in Figure 6, which confirms that the accuracy of the Sudakov approximation at NLO is very high, thereby supporting the usage of EW Sudakov logarithms at NNLO.

Pure EW uncertainties

Assuming that the NLL Sudakov approximation at NNLO is comparably accurate as at NLO, we can consider unknown Sudakov logarithms beyond NNLO as the dominant source of EW uncertainty at high p_{T}. Such $\mathcal{O}(\alpha^3)$ Sudakov terms can be easily estimated via naive exponentiation, which implies the following relations between NLO, NNLO and NNNLO terms,

$$\begin{aligned} \delta^{(2)}_{\text{Sud}} &\simeq \frac{1}{2}\left[\delta^{(1)}_{\text{Sud}}\right]^2, \\ \delta^{(3)}_{\text{Sud}} &\simeq \frac{1}{3!}\left[\delta^{(1)}_{\text{Sud}}\right]^3 \simeq \frac{1}{3}\delta^{(1)}_{\text{Sud}}\,\delta^{(2)}_{\text{Sud}}. \end{aligned} \tag{32}$$

Based on these relations, we estimate the uncertainty due to unknown high-p_{T} EW effects beyond NNLO as

$$\delta^{(1)}\kappa^{(V)}_{\text{nNLO EW}}(x) = \frac{2}{3}\kappa^{(V)}_{\text{NLO EW}}(x)\,\kappa^{(V)}_{\text{NNLO Sud}}(x), \tag{33}$$

which is an approximate implementation of Eq. (32), obtained by neglecting effects from angular integration and multiplying the term $\delta^{(3)}_{\text{Sud}}$ by a factor two, in order to be conservative.

Besides Sudakov exponentiation effects, we introduce a second source of uncertainty, defined, at nNLO EW, as 5% of the absolute full NLO EW correction,

$$\delta^{(2)}\kappa^{(V)}_{\text{nNLO EW}}(x) = 0.05\,|\kappa^{(V)}_{\text{NLO EW}}(x)|. \tag{34}$$

This type of uncertainty has a twofold motivation. At high p_{T}, where Sudakov logarithms dominate, it accounts for unknown terms of order $\alpha^2 \ln^2\left(\frac{Q^2}{M^2}\right)$ that can arise from effects of the form

$$\left(\frac{\alpha}{\pi}\right)^2 \delta^{(1)}_{\text{hard}}\,\delta^{(1)}_{\text{Sud}} = \kappa_{\text{NLO hard}}\,\kappa_{\text{NLO Sud}} \simeq \kappa_{\text{NLO hard}}\,\kappa_{\text{NLO EW}}. \tag{35}$$

Here, in general, the non-Sudakov factor $\kappa_{\text{NLO hard}} = (\frac{\alpha}{\pi})\delta^{(1)}_{\text{hard}}$ can amount to several percent, e.g. due to photon-bremsstrahlung effects in highly exclusive observables. However, for the boson-p_{T} distributions considered in this paper, where dressed leptons are used, the quality of the Sudakov approximation observed in Figure 6 indicates that $\kappa_{\text{NLO hard}}$ is very small. Nevertheless, to be conservative, the uncertainty (34) can accommodate effects as large as $\kappa_{\text{NLO hard}} = 5\%$.

As a second motivation, the uncertainty (34) accounts also for NNLO effects of type $\left(\frac{\alpha}{\pi}\right)^2 \delta^{(2)}_{\text{hard}}$, which can become relevant in the case where hard contributions dominate. In this situation, Eq. (34) amounts to a bound on hard NNLO effects,

$$\left(\frac{\alpha}{\pi}\right)^2 \delta^{(2)}_{\text{hard}} \leq 0.05\, \kappa_{\text{NLO EW}} \simeq 0.05 \left(\frac{\alpha}{\pi}\right) \delta^{(1)}_{\text{hard}}, \tag{36}$$

which corresponds to $\delta^{(2)}_{\text{hard}} \leq \frac{0.05\pi}{\alpha}\delta^{(1)}_{\text{hard}} \simeq 20\, \delta^{(1)}_{\text{hard}}$. This limit should be conservative enough to hold also in situations where the NLO hard correction is accidentally small with respect to its NNLO counterpart.

In order to account for the limitations of the Sudakov approximation at nNLO in a sufficiently conservative way, we introduce an additional source of uncertainty defined as the difference between the rigorous NLL Sudakov approximation (31) and a naive exponentiation of the full NLO EW correction,

$$\delta^{(3)}\kappa^{(V)}_{\text{nNLO EW}}(x) \;=\; \kappa^{(V)}_{\text{NNLO Sud}}(x) - \frac{1}{2}[\kappa^{(V)}_{\text{NLO EW}}(x)]^2. \tag{37}$$

This expression provides an estimate of the typical size of terms of type $\left[\delta^{(1)}_{\text{hard}}\right]^2$ and $\delta^{(1)}_{\text{hard}} \times \delta^{(1)}_{\text{Sud}}$. At NLO EW, defining the uncertainties $\delta^{(i)}\kappa_{\text{NLO EW}}$ in analogy with their nNLO counterparts in Eqs. (33), (34) and (37), we have

$$\begin{aligned}
\delta^{(1)}\kappa^{(V)}_{\text{NLO EW}}(x) &= \frac{2}{2}\left[\kappa^{(V)}_{\text{NLO EW}}(x)\right]^2, \\
\delta^{(2)}\kappa^{(V)}_{\text{NLO EW}}(x) &= 0.05, \\
\delta^{(3)}\kappa^{(V)}_{\text{NLO EW}}(x) &= 0.
\end{aligned} \tag{38}$$

The rough estimate (33) of higher-order EW effects, based on naive exponentiation, can be validated at NLO by comparing the corresponding estimate $\delta^{(1)}\kappa^{(V)}_{\text{NLO EW}}(x)$ against the known NLL Sudakov results at NNLO. This is illustrated in Figure 6, which demonstrates that Eq. (38) (green band) provides a fairly realistic estimate of nNLO EW corrections. The expected effects beyond nNLO, estimated according to Eqs. (33), (34) and (37), turn out to be around $\pm 5\%$ in the multi-TeV tails.

Similarly as for QCD uncertainties, the EW uncertainties in Eqs. (33), (34), (37) and Eq. (38), can be parametrised in terms of nuisance parameters $\vec{\varepsilon}_{\text{EW}}$ and combined via

$$\begin{aligned}
\frac{\mathrm{d}}{\mathrm{d}x}\sigma^{(V)}_{\text{EW}}(\vec{\varepsilon}_{\text{EW}}, \vec{\varepsilon}_{\text{QCD}}) \;=\; & \left[\kappa^{(V)}_{\text{EW}}(x) + \sum_{i=1}^{3} \varepsilon^{(V)}_{\text{EW},i}\, \delta^{(i)}\kappa^{(V)}_{\text{EW}}(x)\right] \\
& \times \frac{\mathrm{d}}{\mathrm{d}x}\sigma^{(V)}_{\text{LO QCD}}(\vec{\varepsilon}_{\text{QCD}}),
\end{aligned} \tag{39}$$

where EW stands for NLO EW or nNLO EW. The nuisance parameters $\varepsilon^{(V)}_{\text{EW},i}$ should be Gaussian distributed with one standard deviation corresponding to the range $\varepsilon^{(V)}_{\text{EW},i} \in [-1, +1]$, and their variations should be applied in a correlated way across p_{T}-bins. Since the first uncertainty (33) reflects the universal exponentiation properties of Sudakov EW

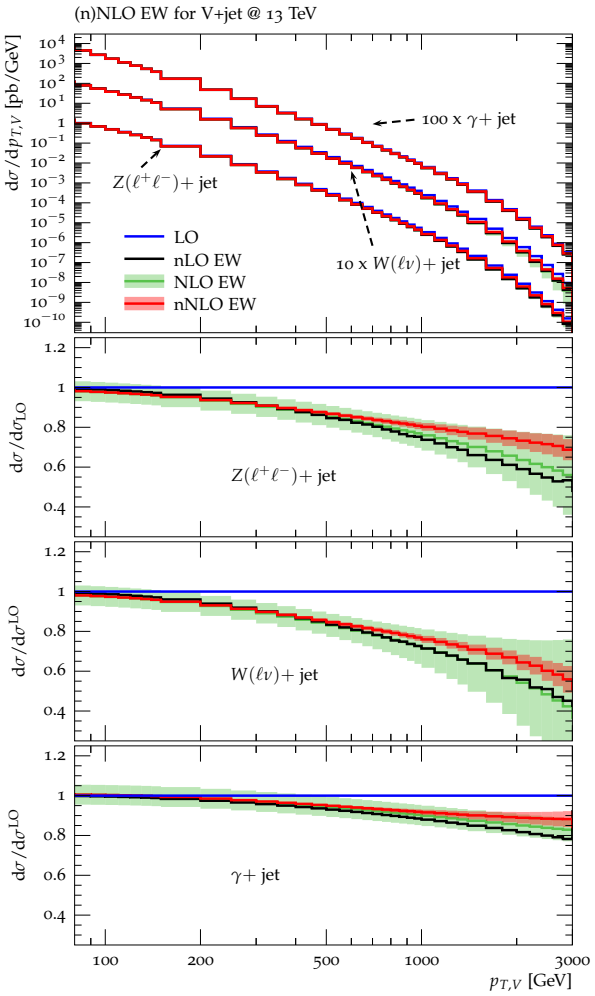

Figure 6: Higher-order EW predictions and uncertainties for different $pp \to V+\text{jet}$ processes at 13 TeV. The main frame displays absolute predictions at LO (blue), NLO EW (green) and nNLO EW (red), as well as NLL Sudakov logarithms at NLO (black), which are denoted as nLO EW. In the ratio plots all results are normalised to LO. Uncertainties at nNLO EW (red band) are evaluated by combining in quadrature the corresponding variations $\delta^{(i)}\kappa^{(V)}_{\text{nNLO EW}}$ as defined in Eqs. (33), (34) and (37) and for $\delta^{(i)}\kappa^{(V)}_{\text{NLO EW}}$ in Eq. (38).

corrections, which permits to predict the magnitude and size of the dominant higher-order corrections for each individual processes, this variation should be correlated across processes, i.e. a single nuisance parameter,

$$\varepsilon^{(W^\pm)}_{\text{EW},1} = \varepsilon^{(Z)}_{\text{EW},1} = \varepsilon^{(\gamma)}_{\text{EW},1} = \varepsilon_{\text{EW},1}, \tag{40}$$

should be used. In contrast, the remaining EW uncertainties (34) and (37) describe subleading NNLO effects whose sign, magnitude and process dependence are unknown. Thus these uncertainties should be treated as uncorrelated, i.e. independent nuisance parameters $\varepsilon^{(V)}_{\text{EW},2}$ and $\varepsilon^{(V)}_{\text{EW},3}$ should be used for each process.

Numerical results

In Figure 6 we show absolute predictions and higher-order EW corrections at NLO and nNLO to the transverse-momentum distribution for the different V+jet processes. Corresponding combined uncertainty estimates according to Eq. (33), Eq. (34), and Eq. (37)

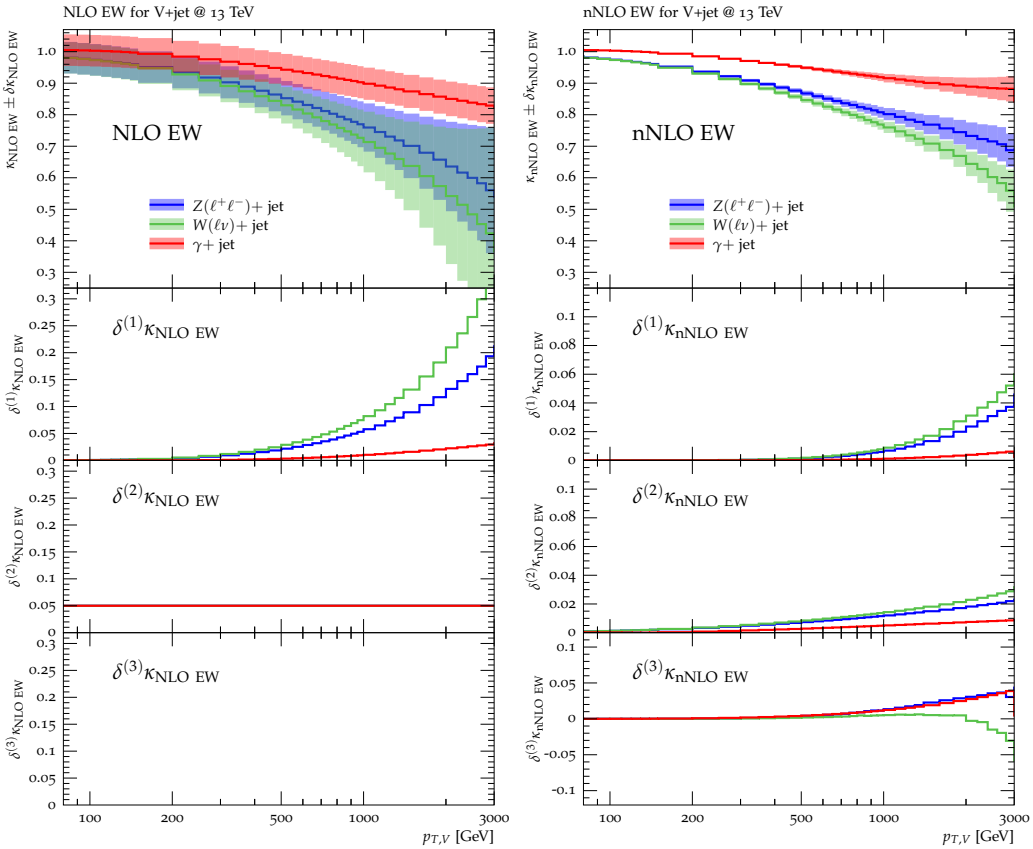

Figure 7: NLO EW (left) and nNLO EW (right) κ-factors for the various $pp \to V+\text{jet}$ processes at 13 TeV. The individual uncertainties $\delta^{(i)}\kappa_{\text{EW}}^{(V)}$ are defined in Eqs. (33), (34) and (37), at nNLO and in Eq. (38) at NLO. The bands in the main frame correspond to their combination in quadrature.

are also shown (in Figure 20 in Appendix B the three EW uncertainties are shown separately). Furthermore, the exact NLO EW corrections are compared to the NLL Sudakov approximation at NLO, denoted as nLO EW.

At large transverse momentum the NLO EW corrections are sizeable. Between p_{T}=1–2 TeV they reach 20–50% for Z+jet and W+jet, and 10–15% for γ+jet. They are partially compensated by the NNLO Sudakov EW corrections, whose size is well covered by the NLO uncertainty $\delta^{(1)}\kappa_{\text{EW}}^{(V)}$. At nNLO the remaining EW uncertainty in W/Z+jet is at the level of a few percent and below one percent for γ+jet. These findings are summarized in Figure 7, where the EW corrections at NLO (left) and nNLO (right) are directly compared for the different processes.

Resulting ratios of p_{T}-distributions for different processes including EW corrections at NLO and nNLO are shown in Figure 8. Here the three types of EW uncertainties are combined in quadrature, while in Figure 21 in Appendix B they are shown separately. In these ratios the uncertainty $\delta^{(1)}\kappa_{\text{EW}}^{(V)}$ is varied in a correlated way between the numerator and denominator, while the effect of $\delta^{(2)}\kappa_{\text{EW}}^{(V)}$ and $\delta^{(3)}\kappa_{\text{EW}}^{(V)}$ in numerator and denominator is added in quadrature. The EW corrections significantly change the shape of the different p_{T}-ratios, with the largest effect observed in the $Z(\ell^+\ell^-)/\gamma$ and W/γ ratios. In these

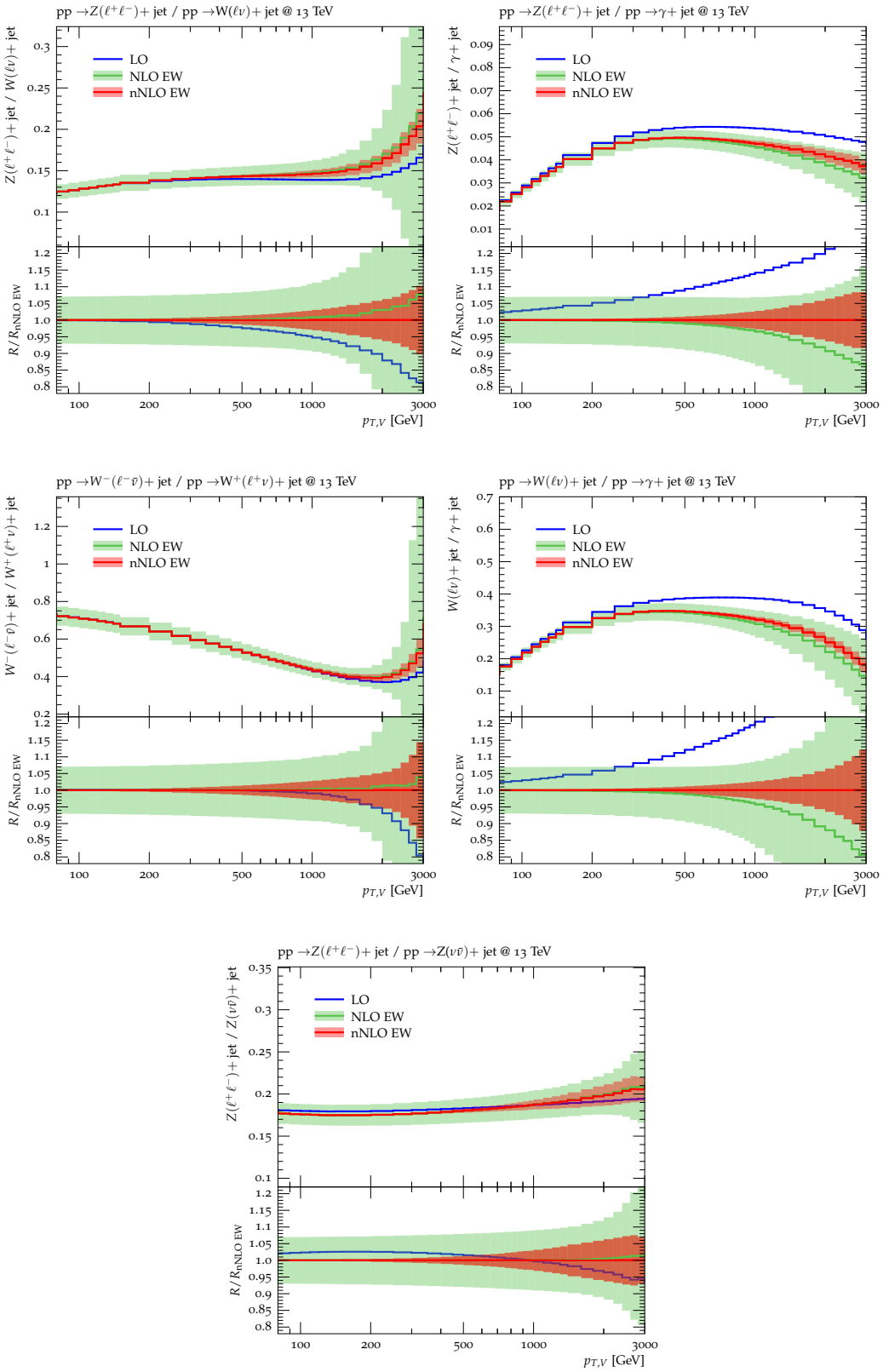

Figure 8: Ratios of p_{T}-distributions for various $pp \to V$+jet processes at LO, NLO EW and nNLO EW accuracy. Relative uncertainties normalised to nNLO EW are illustrated in the lower frames. The bands correspond to a combination (in quadrature) of the three EW uncertainties $\delta^{(i)}\kappa_{\mathrm{EW}}^{(V)}$ defined in Eqs. (33), (34) and (37) at nNLO and in Eq. (38) at NLO. As discussed in the text, the uncertainty $\delta^{(1)}\kappa_{\mathrm{EW}}^{(V)}$ is correlated amongst processes, while $\delta^{(2)}\kappa_{\mathrm{EW}}^{(V)}$ and $\delta^{(3)}\kappa_{\mathrm{EW}}^{(V)}$ are uncorrelated.

ratios the remaining combined EW uncertainties are at the level of few percent in the TeV range, reaching about 5% for $p_{\mathrm{T},V} = 2$ TeV. Interestingly, also the ratios W^-/W^- and $Z(\ell^+\ell^-)/Z(\nu\bar{\nu})$ receive non-negligible EW corrections. In the former ratio these originate from mixed QCD-EW interference contributions, which give relevant (negative) contributions at very high p_{T} in W^++jet production but less in W^-+jet production. The latter ratio receives few percent corrections of QED type.

3.3 Photon-induced production and PDF uncertainties

QED effects associated with the PDFs enter in two ways. Firstly they introduce a photon parton distribution and so open up partonic channels such as $\gamma q \to Vq'$. Secondly they modify the quark (and even gluon PDFs) both through QED effects in the initial conditions and especially in the DGLAP evolution.

Photon-induced $V+$jet production is accounted for by the tervn cim $\frac{\mathrm{d}}{\mathrm{d}x}\sigma^{(V)}_{\gamma-\mathrm{ind.}}$ in eq. (7). It might become relevant in the TeV range, especially in the case of $W+$jet production [19, 20], where the initial-state photon directly couples to a t-channel W. Such contributions are suppressed by a relative factor α/α_S and can be treated at LO, which corresponds to $\gamma q \to Vq$ at $\mathcal{O}(\alpha^2)$ or if necessary at NLO QCD, i.e. up to order $\mathcal{O}(\alpha^2\alpha_{\mathrm{S}})$, which comprises

(b.1) virtual QCD corrections to $\gamma q \to Vq$;

(b.2) $\gamma g \to Vq\bar{q}$ quark bremsstrahlung;

(b.3) $\gamma q \to Vqg$ gluon bremsstrahlung.

The latter can also be understood as photon-induced quark-bremsstrahlung NLO EW contribution to the dominant $q\bar{q}$ channel.

In Figure 9 the impact of LO photon-induced $V+$jet production is illustrated, where effects of the order of 5–10% for W+jet can be observed in the TeV region if `CT14qed_inc` [30] or `LUXqed` PDFs [31] are used. Much larger effects are found with `NNPDF30qed` [32, 33]. The impact of photon-induced production to Z+jet (and also γ+jet) processes on the other hand is negligible [17, 18].

Uncertainties due to photon-induced production can be determined through the intrinsic `LUXqed` PDF uncertainty, given that this includes a model-independent, data-driven determination of the photon distribution. From Figure 9, one sees that these uncertainties are small. Among other recent photon PDFs, `CT14qed_inc` (uncertainties not shown), based on a non-perturbative model with limited data-based constraints for the inelastic contribution, would give somewhat larger uncertainties. `NNPDF30qed` is model-independent and data driven, but uses a different approach from `LUXqed` for deducing the photon distribution from data, which results in large uncertainties in the photon-induced component, of the order of 100% for $pp \to \ell^+\nu_\ell+$jet at $p_{\mathrm{T},\ell} = 1\,\mathrm{TeV}$ [20].

We note that the photon-induced production at LO can be directly included as separate background processes through dedicated MC simulations, in which case they should be excluded for the theoretical predictions in Eq. (7).

Concerning the size of the QED effects on the QCD partons, Figure 10 examines the two main parton luminosities that contribute to the Z+jet process, i.e. $g\Sigma = 2\sum_i(\mathcal{L}_{gq_i} + \mathcal{L}_{g\bar{q}_i})$ (which dominates) and $q\bar{q} = 2\sum_i \mathcal{L}_{q_i\bar{q}_i}$ (which accounts for the remaining 15%−30%). It shows the ratio of these luminosities in `LUXqed_plus_PDF4LHC15_nnlo` relative to the `PDF4LHC15_nnlo` set on which it is based. The ratio is given as a function of half the partonic invariant mass, $M/2$, which is commensurate with the p_{T} of the Z.

Most of the difference between the `LUXqed` set and `PDF4LHC15_nnlo` results in Figure 10 comes from the QED effects in the DGLAP evolution [34], with photon emission during the

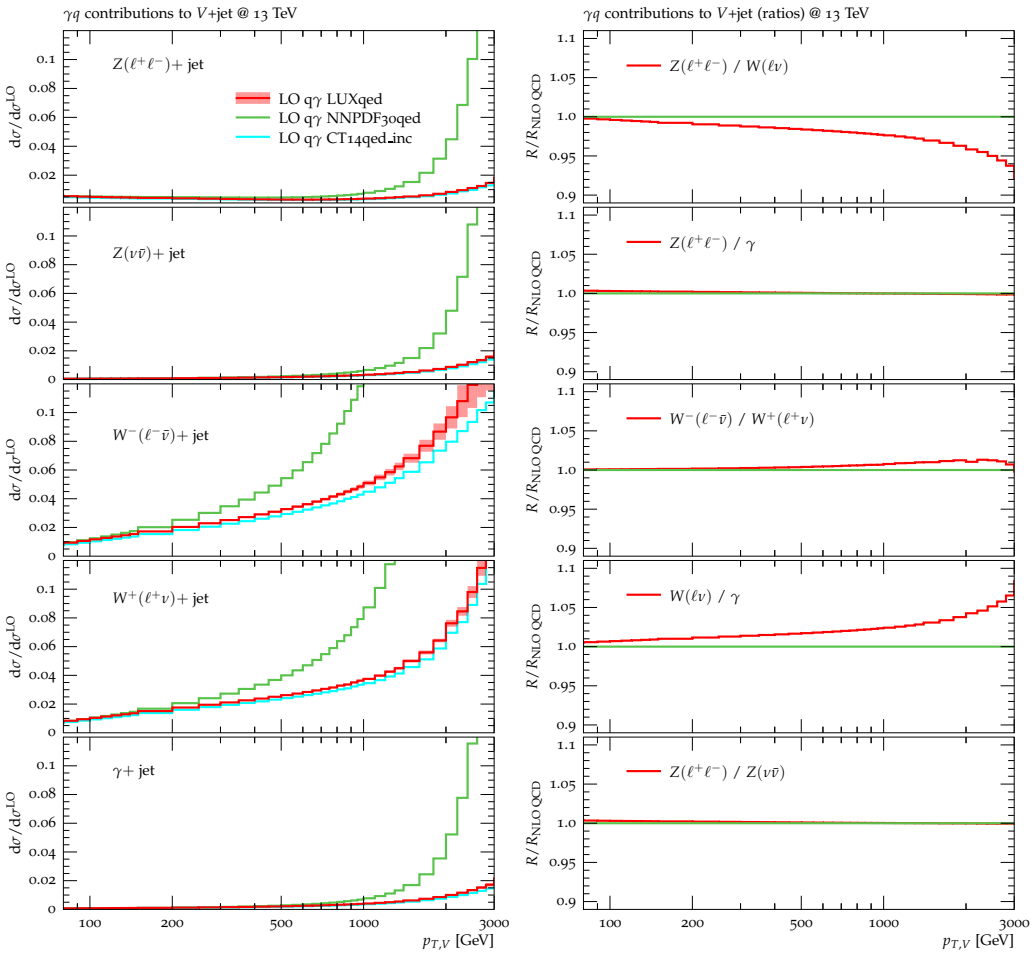

Figure 9: The left plot illustrates the impact of photon-induced contributions relative to $pp \to V+\text{jet}$ at LO for different $V+\text{jet}$ processes. Predictions obtained with `LUXqed`, `CT14qed_inc` and `NNPDF30qed` PDFs are compared. The error band, shown only for the `LUXqed` prediction, reflects PDF uncertainties. The right plot shows, based on `LUXqed` PDFs, $V+$jets ratios at NLO QCD with (red) and without (green) γq-induced contributions at LO.

evolution reducing the momentum in the quarks. This effect reaches about 2% at 2 TeV for the $g\Sigma$ luminosity. There is also a part of the correction associated with the impact of QED effects on the initial partons. In the `LUXqed` set this has been approximated by absorbing the photon momentum from the gluon distribution in `PDF4LHC15_nnlo` and keeping the quarks unchanged at a scale of 10 GeV. This is an ad-hoc procedure, however, insofar as the photon carries only $\simeq 0.3\%$ of the proton momentum (at a scale of 10 GeV), the uncertainty associated with the arbitrariness of this choice should be below 1%.

PDF uncertainties

In addition to QCD and EW uncertainties, also PDF uncertainties should be estimated. Their role can be significant especially at high-p_T, where PDFs tend to be less precise. To indicate how to keep track of PDF effects in the combination of QCD and EW corrections we simply write

$$\vec{\varepsilon}_{\text{QCD}} = (\varepsilon_{\text{QCD},1}, \varepsilon_{\text{QCD},2}, \varepsilon_{\text{QCD},3}, \varepsilon_{\text{PDF},1}, \varepsilon_{\text{PDF},2}, \dots), \tag{41}$$

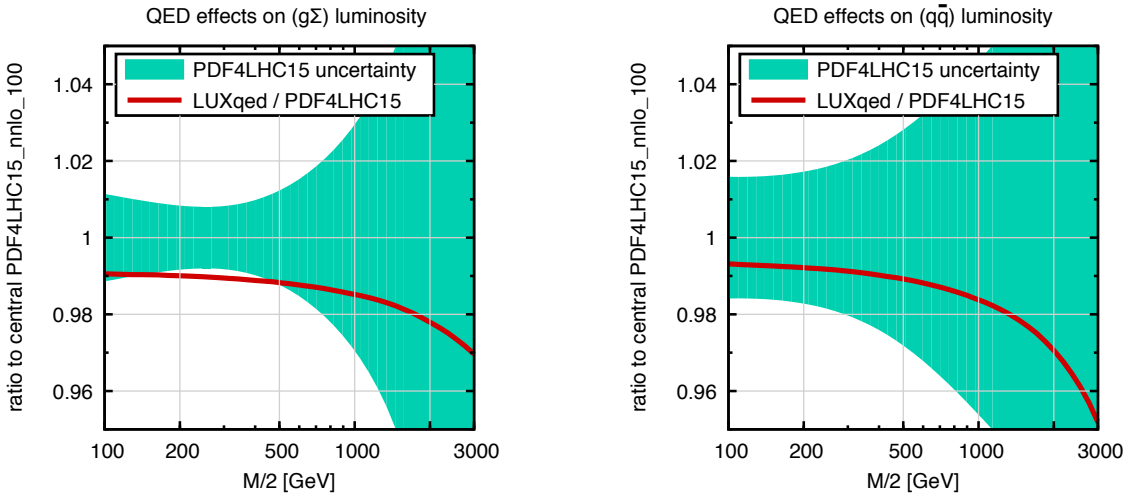

Figure 10: Impact of QED effects on the two partonic luminosities ($g\Sigma$ and $q\bar{q}$) that contribute dominantly to the Z+jet cross section. The luminosity for producing a system of mass M from two flavours a and b is defined as $\mathcal{L}_{ab} = \int_{M^2/s}^1 \frac{dx}{x} f_{a/p}(x, M^2) f_{b/p}(\frac{M^2}{xs}, M^2)$ and the $g\Sigma$ luminosity corresponds to $2\sum_i(\mathcal{L}_{gq_i} + \mathcal{L}_{g\bar{q}_i})$, while the $q\bar{q}$ luminosity corresponds to $2\sum_i \mathcal{L}_{q_i\bar{q}_i}$, where i runs over quark flavours. The solid red lines correspond to the ratio of luminosities obtained with the `LUXqed_plus_PDF4LHC15_nnlo_100` [31] and `PDF4LHC15_nnlo_100` [35] sets, where a given $M/2$ value corresponds roughly to the same $p_{\mathrm{T},Z}$. The bands represent the `PDF4LHC15_nnlo_100` uncertainty, shown for comparison.

meaning that scale variations, process-correlation uncertainties and PDF variations should be applied at the level of QCD calculations and combined with EW corrections on the same footing, as explained in Section 3.5. Rather than giving an explicit definition of the $\varepsilon_{\mathrm{PDF},i}$'s, for details of the implementation we simply refer to the PDF4LHC recommendation [35]. PDF variations should be applied in a fully correlated way across processes and p_{T} bins.

In Figure 11 we illustrate the effect of PDF uncertainties within `LUXqed` (for the quark and gluon uncertainties based on `PDF4LHC15_nnlo_100`) for the different V+jets processes and process ratios at NLO QCD. Up to about 800 GeV the PDF uncertainties on the nominal p_{T} distributions remain below 2%. In the tails of the distributions the PDF uncertainties significantly increase. They grow beyond 5% for $p_{\mathrm{T}} \gtrsim 1.5$ TeV. In the Z/W ratio the PDF uncertainties cancel almost completely and remain below 0.5(2)% up to $p_{\mathrm{T}} \approx 800(1500)$ GeV. In the Z/γ and W/γ ratios the PDF uncertainties are at the level of $1-2\%$ up to $p_{\mathrm{T}} \approx 1300$ GeV, while the W^-/W^+ ratio is subject to PDF uncertainties beyond 5% already for $p_{\mathrm{T}} \gtrsim 1$ TeV, driven by uncertainties on the u/d-ratio at large Bjorken-x [3].

3.4 Real-boson emission

Inclusive diboson production (in particular $pp \to VV'$+jets) can be understood as the real-emission counterpart to NLO EW corrections to $pp \to V+$jet. Both contributions are separately finite and well defined if $V' = W, Z$. Although they are expected to cancel against each other to a certain (typically little) extent, in practice one should only make sure that both types of processes, $V+$jets and VV'(+jets), are included in the analysis, and, in order to avoid double counting, contributions of type VV'(+jets) should be included in separate diboson MC samples and not as EW correction effects in $V+$jets samples. Unless a very strong cancellation is observed (which is typically not the case), there is no reason to worry about the possible correlation of uncertainties in $V+$jets and VV'(+jets)

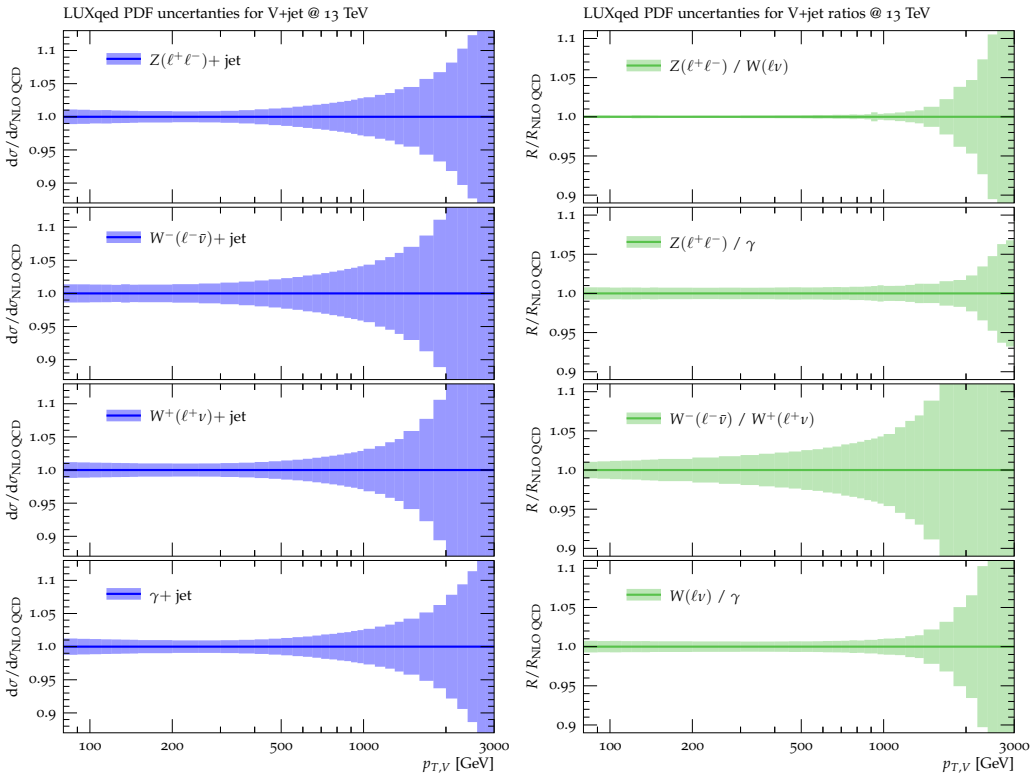

Figure 11: Relative `LUXqed_plus_PDF4LHC15_nnlo_100` PDF uncertainties on the nominal p_T distributions for the different $pp \to V+$jet processes at 13 TeV evaluated to NLO QCD are shown on the left. Corresponding PDF uncertainties for $V+$ jet ratios are shown on the right. In the ratios different PDF replicas are correlated across processes and the resulting errors on the respective ratio are combined in quadrature.

production, i.e. one can treat the respective uncertainties as uncorrelated.

As concerns the accuracy of MC simulations of $pp \to VV'(+\text{jets})$, it is important to notice that a large diboson background to inclusive vector-boson production at high p_T is expected to arise from $pp \to VV'j$ topologies with a hard back-to-back Vj system accompanied by a relatively soft extra vector boson. This calls for a reliable description of $VV'+$ jet including QCD (and possibly EW) corrections. Thus we recommend the use of merged diboson samples that include at least one extra jet at matrix-element level. At the TeV scale, the EW corrections to $pp \to VV'+$ jet can become quite large [36, 37] and should ultimately be included, together with the corresponding QCD corrections [38–45].

3.5 Combination of QCD and electroweak corrections

The combination (7) of higher-order predictions presented in the previous sections can be cast in the form,

$$\frac{\mathrm{d}}{\mathrm{d}x}\sigma^{(V)}_{\mathrm{TH}}(\vec{\mu}) \;=\; K^{(V)}_{\mathrm{TH}}(x,\vec{\mu})\,\frac{\mathrm{d}}{\mathrm{d}x}\sigma^{(V)}_{\mathrm{LO\,QCD}}(\vec{\mu}_0) + \frac{\mathrm{d}}{\mathrm{d}x}\sigma^{(V)}_{\gamma-\mathrm{ind.}}(x,\vec{\mu}), \tag{42}$$

where

$$K^{(V)}_{\mathrm{TH},\oplus}(x,\vec{\mu}) \;=\; K^{(V)}_{\mathrm{N^kLO}}(x,\vec{\mu}) + \kappa^{(V)}_{\mathrm{EW}}(x)\,K^{(V)}_{\mathrm{LO}}(x,\vec{\mu}) \tag{43}$$

corresponds to the standard additive combination of QCD and EW corrections as defined in Eq. (9) and Eqs. (23)–(25). Note that the scale-dependent LO QCD K-factor in Eq. (43)

is due to the fact that QCD and EW correction factors are normalised to $\sigma^{(V)}_{\text{LO QCD}}(\vec{\mu}_0)$ and $\sigma^{(V)}_{\text{LO QCD}}(\vec{\mu})$, respectively.

Mixed QCD–EW corrections of relative $\mathcal{O}(\alpha\alpha_S)$ are not known to date. However, in order to obtain an improved prediction that partially includes such mixed effects, higher-order EW and QCD corrections can be combined through a factorised prescription[8],

$$K^{(V)}_{\text{TH},\otimes}(x,\vec{\mu}) \;=\; K^{(V)}_{\text{N}^k\text{LO}}(x,\vec{\mu})\left[1+\kappa^{(V)}_{\text{EW}}(x)\right]. \tag{44}$$

This form is motivated by the known factorisation of QCD corrections from the large Sudakov-enhanced EW corrections at high energies. Moreover, in cases where the multiplicative and additive approach are far apart from each other, for instance in the presence of giant K-factors [19, 49], we know that the former is much more reliable. The difference between additive and multiplicative combination of QCD and EW corrections is twofold. On the one hand, the multiplicative prescription (44) leads to mixed terms of relative $\mathcal{O}(\alpha\alpha_S)$ that can become sizeable when QCD and EW corrections are simultaneously enhanced. On the other hand, irrespectively of the size of QCD corrections, when EW corrections are large the additive approach (43) leads to a significant growth of scale uncertainties as compared to NLO QCD. In contrast, since the relative EW correction factors $\kappa^{(V)}_{\text{EW}}(x)$ are essentially insensitive to QCD scale variations, combining EW and QCD corrections in the multiplicative approach (44) results in the same scale dependence as for pure QCD predictions.

Useful insights into the typical size of mixed EW–QCD NNLO corrections to $pp \to V+\text{jet}$ can be gained by studying the NLO EW corrections to $pp \to V+2\,\text{jets}$ [19, 50], which enter at the same order and represent the real–virtual part of the full NNLO mixed corrections. In particular, the differences between NLO EW K-factors for $V+\text{jet}$ and $V+2\,\text{jets}$, shown in Figure 12 for $pp \to Z/W+1,2\,\text{jets}$, can provide a quantitative estimate of non-factorising NNLO mixed corrections. It turns out that the correspondence between EW K-factors for different jet multiplicities[9] provides strong support for the hypothesis of EW–QCD factorisation.

QCD-EW combination with uncertainties of relative $\mathcal{O}(\alpha\alpha_S)$

Based on the above observations, we recommend to combine QCD and EW corrections according to the multiplicative prescription (44), while the difference with respect to the additive approach (43) can be used as input in order to model the uncertainty due to non-factorised mixed EW–QCD effects. Thus, including QCD+EW predictions and related uncertainties as specified in Eq. (21) and Eq. (39), we define

$$\begin{aligned}
K^{(V)}_{\text{TH}}(x,\vec{\varepsilon}_{\text{QCD}},\vec{\varepsilon}_{\text{EW}},\varepsilon_{\text{mix}}) &= K^{(V)}_{\text{TH},\otimes}(x,\vec{\varepsilon}_{\text{QCD}},\vec{\varepsilon}_{\text{EW}}) + \varepsilon_{\text{mix}}\,\delta K^{(V)}_{\text{mix}}(x) \\
&= \left[K^{(V)}_{\text{N}^k\text{LO}}(x) + \sum_{i=1}^{3}\varepsilon_{\text{QCD},i}\,\delta^{(i)}K^{(V)}_{\text{N}^k\text{LO}}(x)\right] \\
&\quad\times\left[1+\kappa^{(V)}_{\text{EW}}(x) + \sum_{i=1}^{3}\varepsilon^{(V)}_{\text{EW},i}\,\delta^{(i)}\kappa^{(V)}_{\text{EW}}(x)\right] + \varepsilon_{\text{mix}}\,\delta K^{(V)}_{\text{mix}}(x),
\end{aligned} \tag{45}$$

where the mixed EW–QCD uncertainty reads

$$\delta K^{(V)}_{\text{mix}}(x) \;=\; 0.1\left[K^{(V)}_{\text{TH},\oplus}(x,\vec{\mu}_0) - K^{(V)}_{\text{TH},\otimes}(x,\vec{\mu}_0)\right], \tag{46}$$

[8] See, e.g. Refs. [46–48] for a factorised treatment of QCD and EW corrections for Higgs-strahlung and vector-boson fusion processes.

[9] To be precise, above 1 TeV we observe small deviations of 1–3%. In the case of $pp \to W+\text{jet}$, such effects are due to mixed EW–QCD interference contributions of $\mathcal{O}(\alpha_S\alpha^2)$ in channels of type $qq \to qqW$ (see the difference between red and magenta curves in Figure 12).

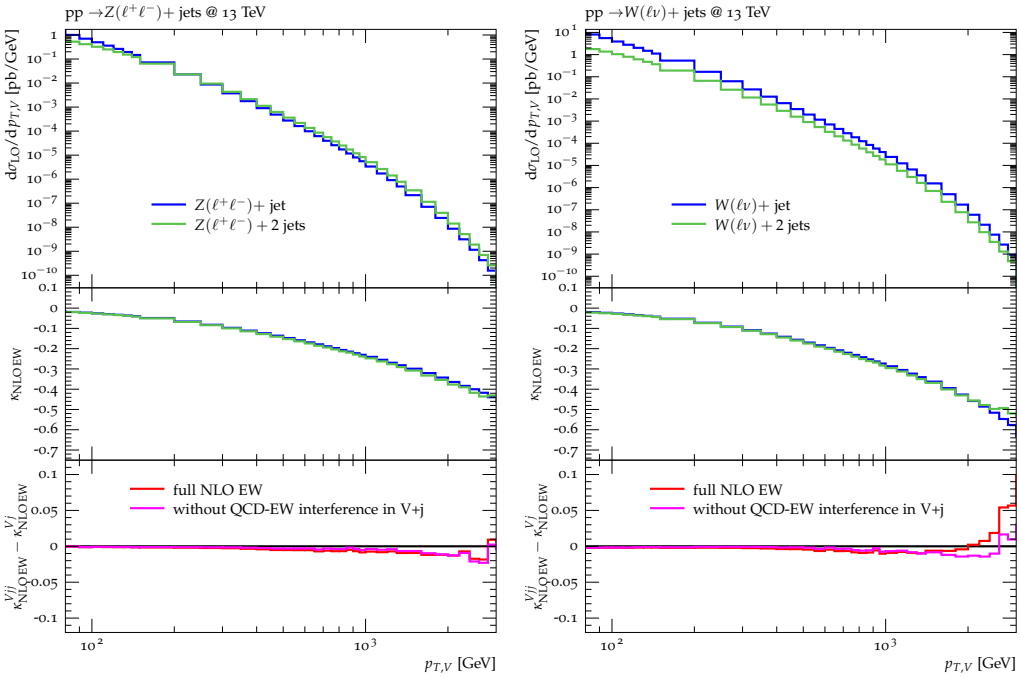

Figure 12: NLO EW predictions for the production of $Z(\ell^+\ell^-)$+jets (left) and $W^\pm(\ell\nu)$+jets (right) at 13 TeV. The NLO EW corrections for $pp \to V + 1\,\text{jet}$ (blue) and $pp \to V + 2\,\text{jets}$ are compared (green). In the $V + 2\,\text{jet}$ predictions we require, besides the inclusive event selection detailed in Section 4, at least two anti-k_T jets with $R = 0.4$ and $p_T > 30$ GeV (without any η cuts). The lower ratio plot shows the difference in the EW corrections between the one- and two-jet processes, $\Delta\kappa_{\text{NLO EW}} = \kappa^{Vjj}_{\text{NLO EW}} - \kappa^{Vj}_{\text{NLO EW}}$ for the full NLO EW corrections (red) and excluding the finite mixed QCD-EW bremsstrahlung interference contributions to $pp \to V + 1\,\text{jet}$ (magenta).

and the related nuisance parameter should be Gaussian distributed with one standard deviation corresponding to the range $\varepsilon_\text{mix} \in [-1, +1]$. This rather small value of the factor 0.1 in Eq. (46) reflects the high degree of EW–QCD factorisation observed in Figure 12. Variations of ε_mix should be correlated across different processes.

In Figure 13 the difference between the additive and the multiplicative combination of QCD and EW corrections together with the corresponding uncertainty estimate (46) is shown for the various V+jet processes.

4 Setup for numerical predictions

In this section we define physics objects (Section 4.1), acceptance cuts and observables (Section 4.2), input parameters (Section 4.3) and tools (Section 4.4) used in the theoretical calculations for $pp \to W^\pm/Z/\gamma+\,\text{jet}$.

The definitions of physics objects, cuts and observables—which specify the setup for the reweighting procedure discussed in Section 2—should be adopted both for theoretical calculations and for their Monte Carlo counterpart in the reweighting factor (3). The details of the reweighting setup are designed such as to avoid any possible deficit in the perturbative predictions (e.g. due to lack of resummation at small p_T) and any bias due to non-perturbative aspects of Monte Carlo simulations (e.g. leptons and missing energy from hadron decays). Let us also recall that this setup is completely independent of the physics objects, cuts and observables employed in the experimental analyses.

As concerns input parameters and PDFs, the recommendation of Section 4.3 should be

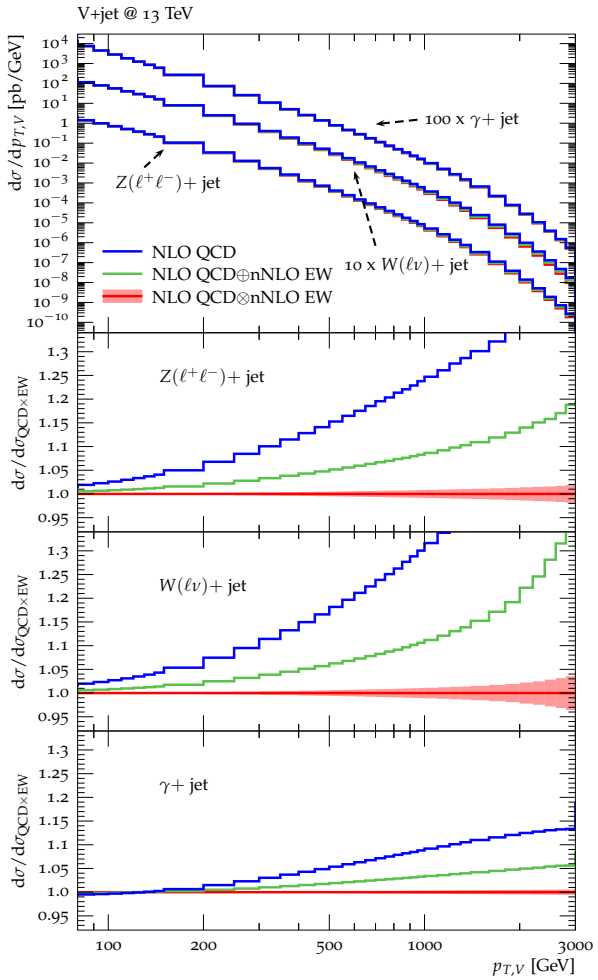

Figure 13: Comparison of additive (green) and multiplicative (red) combination of NLO QCD and nNLO EW corrections for various $pp \to V+$jet processes at 13 TeV. The red band corresponds to the mixed QCD–EW uncertainty (46). The NLO QCD result without EW corrections is shown in blue.

applied to all QCD and EW higher-order calculations. In particular, it is mandatory to compute (N)NLO QCD and EW corrections in the same EW input scheme, otherwise NLO EW accuracy would be spoiled. Instead, Monte Carlo simulations and the corresponding $\frac{\mathrm{d}}{\mathrm{d}x}\sigma^{(V)}_{\mathrm{MC}}$ contributions to the reweighting factor (3) do not need to be based on the same input parameters and PDFs used for theory predictions.

We recommend handling $W/Z+$jet production and decay on the Monte Carlo side as the full processes $pp \to \ell\ell/\ell\nu/\nu\nu+$jet, i.e. with a consistent treatment of off-shell effects, as is done on the theory side.

4.1 Definition of physics objects

In the following we define the various physics objects relevant for higher-order perturbative calculations and for the reweighting in the Monte Carlo counterparts in Eq. (3).

Neutrinos

In parton-level calculations of $pp \to \ell\ell/\ell\nu/\nu\nu+$jet, neutrinos originate only from vector-boson decays, while in Monte Carlo samples they can arise also from hadron decays. In

order to avoid any bias in the reweighting procedure, only neutrinos arising from Z and W decays at Monte Carlo truth level should be considered.

Charged leptons

Distributions in the lepton p_{T} and other leptonic observables are known to be highly sensitive to QED radiative corrections, and the differences in the treatment of QED radiation on Monte Carlo and theory side can lead to a bias in the reweighting procedure. This should be avoided by using dressed leptons, i.e. recombining all leptons with nearly collinear photons that lie within a cone

$$\Delta R_{\ell\gamma} = \sqrt{\Delta\phi_{\ell\gamma}^2 + \Delta\eta_{\ell\gamma}^2} < R_{\mathrm{rec}}. \tag{47}$$

For the radius of the recombination cone we employ the standard value $R_{\mathrm{rec}} = 0.1$, which allows one to capture the bulk of the collinear final-state radiation, while keeping contamination from large-angle photon radiation at a negligible level. All lepton observables as well as the kinematics of reconstructed W and Z bosons are defined in terms of dressed leptons, and, in accordance with standard experimental practice, both muons and electrons should be dressed. In this way differences between electrons and muons become negligible, and the reweighting function needs to be computed only once for a generic lepton flavour ℓ.

Similarly as for neutrinos, only charged leptons that arise from Z and W decays at Monte Carlo truth level should be considered. Concerning QCD radiation in the vicinity of leptons, no lepton isolation requirement should be imposed in the reweighting procedure. In the experimental analysis lepton isolation cuts can be applied in the usual manner.

Z and W bosons

The off-shell four-momenta of W and Z bosons are defined as

$$p_{W^+}^\mu = p_{\ell^+}^\mu + p_{\nu_\ell}^\mu, \qquad p_{W^-}^\mu = p_{\ell^-}^\mu + p_{\bar{\nu}_\ell}^\mu, \tag{48}$$

$$p_Z^\mu = p_{\ell^+}^\mu + p_{\ell^-}^\mu, \qquad p_Z^\mu = p_{\nu_\ell}^\mu + p_{\bar{\nu}_\ell}^\mu, \tag{49}$$

where the leptons and neutrinos that result from Z and W decays are defined as discussed above.

Photons

At higher orders in QCD, photon production involves final-state $q \to q\gamma$ splittings that lead to collinear singularities when QCD radiation is emitted in the direction of the photon momentum. Since such singularities are of QED type, they are not cancelled by corresponding virtual QCD singularities. Thus, in order to obtain finite predictions in perturbation theory, the definition of the $pp \to \gamma+$ jet cross section requires a photon-isolation prescription that vetoes collinear $q \to q\gamma$ radiation while preserving the cancellation of QCD infrared singularities.

To this end, in this study we adopt Frixione's isolation prescription [51], which limits the hadronic transverse energy within a smooth cone around the photon by requiring

$$\sum_{i=\text{partons/hadrons}} p_{\mathrm{T,i}}\,\Theta(R - \Delta R_{i\gamma}) \leq \epsilon_0\, p_{\mathrm{T},\gamma} \left(\frac{1-\cos R}{1-\cos R_0}\right)^n \quad \forall\, R \leq R_0, \tag{50}$$

where the sum runs over all quarks/gluons and hadrons at parton level and Monte Carlo level, respectively, while $p_{\mathrm{T,i}}$ and $p_{\mathrm{T},\gamma}$ denote the transverse momenta of partons/hadrons

and photons. The p_{T}-fraction ε_0, the cone size R_0, and the exponent n are free parameters that allow one to control the amount of allowed QCD radiation in the vicinity of the photon.

The photon-isolation prescription is applicable to QCD as well as to EW higher-order corrections. At NLO EW, $\gamma+$ jet production involves bremsstrahlung contributions with two final-state photons. In this case, at least one isolated photon is required. The other photon might become soft, guaranteeing cancellation of related soft and collinear singularities in the virtual EW corrections. In case of two isolated photons in the final state, the hardest photon is considered. In particular, an explicit photon isolation prescription is mandatory at NLO EW in order to prevent uncancelled singularities from $q \to q\gamma$ splittings in the $\mathcal{O}(\alpha^2\alpha_{\mathrm{S}})$ mixed EW–QCD contributions from $qq \to qq\gamma$ and crossing-related channels.

As a consequence of $q \to q\gamma$ collinear singularities and the need to apply a photon isolation prescription, QCD corrections to $pp \to \gamma+$ jet behave differently as compared to $Z/W+$ jet production. A quantitative understanding of this difference and its implications on the correlation of QCD uncertainties between $\gamma+$ jet and $Z+$ jet production is crucial for the extrapolation of $\gamma+$ jet measurements to $Z+$ jet dark-matter backgrounds. At the TeV scale, where $p_{\mathrm{T},V} \gg M_{W,Z}$, one might naively expect that differences between massive and massless vector bosons tend to disappear from the viewpoint of QCD dynamics. However, the presence of collinear $q \to qV$ singularities at (N)NLO QCD implies a logarithmic sensitivity to the vector-boson masses, which results, respectively in $\ln(p_{\mathrm{T},V}/M_V)$ and $\ln(R_0)$ terms for the case of massive vector bosons and photons.

As discussed in Section 3, in order to quantify the correlation of QCD uncertainties across different $V+$ jet processes, we propose a systematic approach to isolate QCD effects that are process independent (at large $p_{\mathrm{T},V}$) from $\gamma+$ jet specific ones. To this end we introduce a modified photon isolation prescription, which is designed such as to render the QCD dynamics of $\gamma+$ jet and $Z/W+$ jet production as similar as possible at high p_{T}. To this end we introduce a dynamic cone radius

$$R_{\mathrm{dyn}}(p_{\mathrm{T},\gamma}, \varepsilon_0) = \frac{M_Z}{p_{\mathrm{T},\gamma}\sqrt{\varepsilon_0}}, \tag{51}$$

which is chosen in such a way that the invariant mass of a photon-jet pair with $R_{\gamma j} = R_{\mathrm{dyn}}$ and $p_{\mathrm{T},j} = \varepsilon_0\, p_{\mathrm{T},\gamma}$ corresponds to the Z-boson mass, i.e.

$$M_{\gamma j}^2 \simeq p_{\mathrm{T},\gamma}\, p_{\mathrm{T},j} R_{\gamma j}^2 = \varepsilon_0\, p_{\mathrm{T},\gamma}^2 R_{\mathrm{dyn}}^2 = M_Z^2, \tag{52}$$

where the first identity is valid in the small-R approximation. In this way, using a smooth isolation with $R_0 = R_{\mathrm{dyn}}(p_{\mathrm{T},\gamma}, \varepsilon_0)$ mimics the role of the Z- and W-boson masses as regulators of collinear singularities in $Z/W+$jet production at high p_{T}, while using a fixed cone radius R_0 would correspond to an effective $M_{\gamma j}$ cut well beyond $M_{Z,W}$, resulting in a more pronounced suppression of QCD radiation in $\gamma+$ jet production as compared to $Z/W+$ jet.

Specifically, as default photon selection for the theoretical predictions[10] in this study we use the dynamic cone isolation defined through Eq. (50) and Eq. (51), with parameters

$$\varepsilon_{0,\mathrm{dyn}} = 0.1, \qquad n_{\mathrm{dyn}} = 1, \qquad R_{0,\mathrm{dyn}} = \min\left\{1.0, R_{\mathrm{dyn}}(p_{\mathrm{T},\gamma}, \varepsilon_{\mathrm{dyn},0})\right\}. \tag{53}$$

Note that, in order to prevent that the veto against collinear QCD radiation is applied to an excessively large region of phase space, the dynamic cone radius in Eq. (53) is limited to $R_{\mathrm{dyn}} \leq 1.0$. As a result of this upper bound, for $p_{\mathrm{T},\gamma} < M_Z \varepsilon_{0,\mathrm{dyn}}^{-1/2} \simeq 290\,\mathrm{GeV}$ the cone radius

[10] The same isolation prescription used for theory predictions should be applied also to their MC counterparts $\mathrm{d}\sigma_{\mathrm{MC}}/\mathrm{d}x$ in the context of the reweighting procedure.

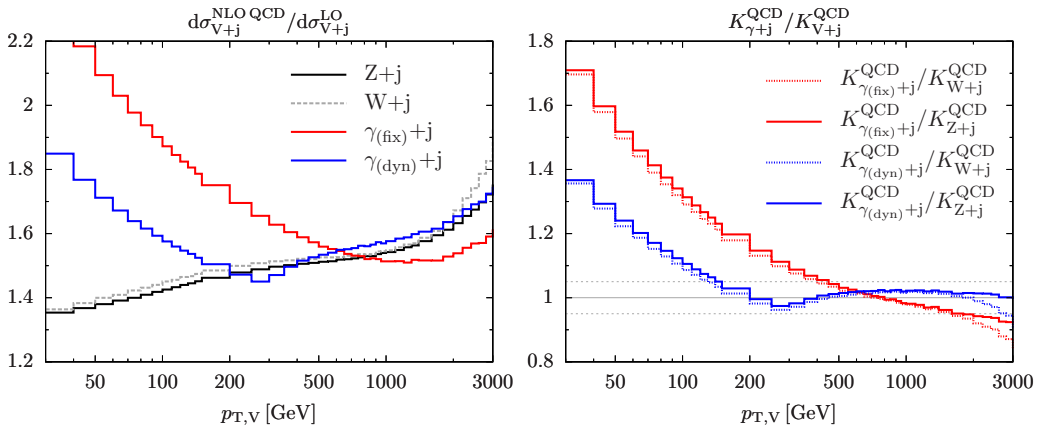

Figure 14: Comparison of NLO QCD K-factors (left) for $W+$jet, $Z+$jet, and $\gamma+$jet production with dynamic photon isolation (53) and standard fixed-cone isolation (54). On the right corresponding ratios of K-factors are shown.

is kept fixed, and the impact of collinear QCD radiation starts to be significantly enhanced as compared to the case of $Z/W+$jet production. Vice versa, for $p_{T,\gamma} > M_Z \varepsilon_{0,\mathrm{dyn}}^{-1/2}$, thanks to the dynamic isolation cone (53), QCD effects in $\gamma+$jet and $Z/W+$jet production become closely related, and the degree of correlation between QCD uncertainties across all $V+$jet processes can be described with the prescription of Eqs. (19)–(20).

For a realistic assessment of theoretical uncertainties, one should also consider the fact that photon isolation prescriptions used in experimental analyses differ in a significant way from the dynamic prescription of Eq. (53). To this end, we recommend to repeat the reweighting procedure using theory predictions for $\gamma+$jet based on a standard Frixione isolation (50) with fixed cone radius and parameters that mimic typical experimental selections at particle level [52],

$$\varepsilon_{0,\mathrm{fix}} = 0.025, \qquad n_{\mathrm{fix}} = 2, \qquad R_{0,\mathrm{fix}} = 0.4. \tag{54}$$

The difference between $\gamma+$jet MC samples reweighted in the dynamic- and fixed-cone setup should be taken as an additional uncertainty for $pp \to \gamma+$jet.

As ingredients for this uncertainty estimate, besides a full set of $pp \to \gamma+$jet predictions and uncertainties with dynamic photon isolation, we provide nominal predictions (without uncertainties) with fixed-cone isolation (54) (see Appendix A). A comparison of the various $V+$jet K-factors at NLO QCD with dynamic and fixed cone isolation is shown in Figure 14.

Predictions for $\gamma+$jet at (n)NLO EW are based on the dynamical cone prescription (53). Here, differences with respect to the fixed-cone isolation (54) are well below the percent level.

QCD partons and photons inside jets

In order to avoid any bias due to the different modelling of jets in MC simulations and perturbative calculations, theory calculations and reweighting should be performed at the level of inclusive vector-boson p_T distributions, without imposing any requirement on the recoiling jet(s). Predictions presented in this study are thus independent of specific jet definitions or jet cuts.

Concerning the composition of the recoil, we observe that, at NLO EW, $q \to q\gamma$ splittings can transfer an arbitrary fraction of the recoiling momentum from QCD partons to photons. In particular, in $pp \to V\gamma j$ contributions of $\mathcal{O}(\alpha^2\alpha_S)$, the photon can carry up to 100% of the recoil momentum. Such contributions involve soft QCD singularities that are cancelled by including also virtual QCD corrections to $pp \to V\gamma$. In order to minimise

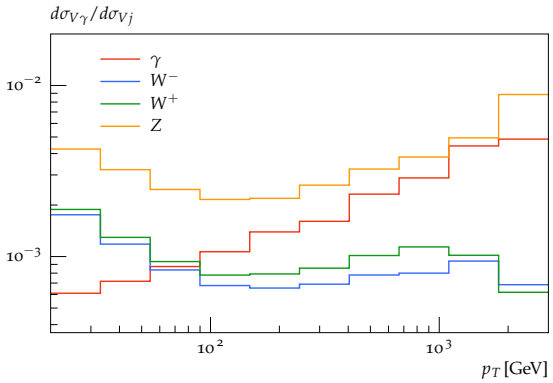

Figure 15: Ratios of distributions in the vector-boson transverse momenta for $pp \to V\gamma$ versus $pp \to Vj$ at LO with $\mu_{\mathrm{R,F}} = H_{\mathrm{T}}/2$. The vector bosons $V = W^{\pm}, Z, \gamma$ are on shell and $\sqrt{s} = 13\,\mathrm{TeV}$.

double counting with diboson production,[11] $V\gamma$ production at LO is not included in the EW corrections to $pp \to Vj$. In practice, as demonstrated in Figure 15, the relative weight of $pp \to V\gamma$ at $\mathcal{O}(\alpha^2)$ versus $pp \to Vj$ at $\mathcal{O}(\alpha\alpha_{\mathrm{S}})$ is well below the percent level. Thus the impact of $\mathcal{O}(\alpha^2\alpha_{\mathrm{S}})$ contributions from hard $V\gamma$ production, which are included in this study, should be completely negligible.

4.2 Cuts and observables

The reweighting should be performed in a fully inclusive $V+$jet setup, imposing a single cut

$$p_{\mathrm{T},V} > 30\,\mathrm{GeV} \quad \text{for} \quad V = W^{\pm}, Z, \gamma, \tag{55}$$

with $p_{\mathrm{T},W^{\pm}}$ and $p_{\mathrm{T},Z}$ defined as in Section 4.1. The cut (55) is crucial in order to avoid the region where perturbative predictions suffer form the lack of QCD resummation.[12]

For leptons and MET we do not apply any p_{T} or rapidity cuts. Moreover, we do not impose any restrictions on QCD radiation in the vicinity of leptons and MET. Also QCD radiation is handled in a fully inclusive way, i.e. the presence of a recoiling jet is not explicitly required, and, as discussed in Section 4.1, at NLO EW the recoil can be entirely carried by a photon. Here we want to stress again that of course the particle-level analysis of the reweighted Monte Carlo samples can (and will) involve a more exclusive event selection than used for the reweighting itself.

The differential distributions to be used for the reweighting of the various $pp \to V+$jet processes and process-specific selection cuts to be applied in addition to Eq. (55) are summarised in Table 1. In the case of $pp \to \nu\bar{\nu}+$jet all three neutrino species are added, while for all other Z and W decays only a single lepton generation is considered. For $pp \to \ell^+\ell^-+$jet an extra invariant-mass cut is applied in order to avoid far off-shell contributions, especially from $\gamma^* \to \ell^+\ell^-$ at low invariant mass. The relatively low value of the lower cut, $m_{\ell\ell} > 30\,\mathrm{GeV}$, is intended to minimise cross section loss due to photon radiation that shifts events from the Z-peak region down to lower invariant mass (see Figure 16). This choice guarantees a reduced sensitivity with respect to the modelling of QED radiation.

The following binning is adopted for distributions in the reconstructed vector-boson

[11] Diboson backgrounds, including $pp \to V\gamma$, can be included through separate Monte Carlo samples in the experimental analyses.

[12] See e.g. the comparison of NNLOPS against fixed-order predictions in Figure 3 of Ref. [53].

process	extra cuts	observable	comments
$pp \to \ell^+\nu_\ell + \text{jet}$	none	$p_{\text{T},\ell^+\nu_\ell}$	$\ell = e$ or μ
$pp \to \ell^-\bar{\nu}_\ell + \text{jet}$	none	$p_{\text{T},\ell^-\bar{\nu}_\ell}$	$\ell = e$ or μ
$pp \to \nu_\ell\bar{\nu}_\ell + \text{jet}$	none	$p_{\text{T},\nu_\ell\bar{\nu}_\ell}$	$\ell = e + \mu + \tau$
$pp \to \ell^+\ell^- + \text{jet}$	$m_{\ell\ell} > 30\,\text{GeV}$	$p_{\text{T},\ell^+\ell^-}$	$\ell = e$ or μ
$pp \to \gamma + \text{jet}$	dynamic isolation (51)–(53)	$p_{\text{T},\gamma}$	

Table 1: Extra selection cuts, in addition to Eq. (55), and observables for the various $V+\text{jet}$ processes. Alternative predictions for γ+jet production are provided also for the case of a standard Frixione isolation with parameters (54).

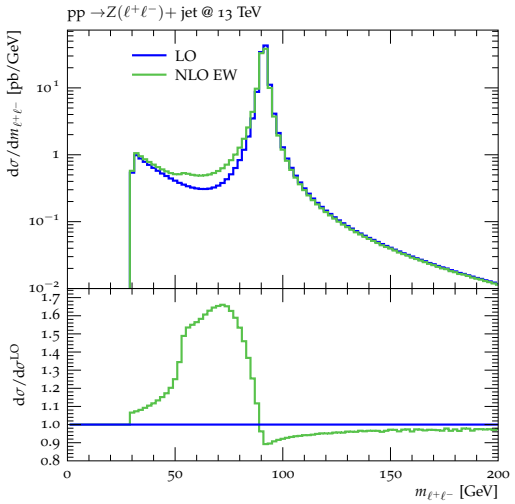

Figure 16: Dilepton invariant-mass distribution in $pp \to \ell^+\ell^-$+jet for $m_{\ell\ell} \in [30, 200]\,\text{GeV}$ comparing LO and NLO EW. Collinear lepton–photon pairs with $R_{\gamma\ell} < 0.1$ are recombined.

transverse momenta,

$$\frac{p_\text{T}}{\text{GeV}} \in [30, 40, \ldots, 140, 150, 200, 250 \ldots, 950, 1000, 1100, 1200, 1300, 1400, 1600 \ldots, 2800, 3000, 6500]\,. \tag{56}$$

4.3 Input parameters, PDFs and QCD scales

Input parameters and PDFs employed for theoretical predictions in this study are specified in the following. Let us recall that, as discussed in Section 2, Monte Carlo samples used in the experimental analyses do not need to be generated with the same input parameters and PDFs used for higher-order theoretical predictions.

In the calculation of $pp \to \ell\ell/\ell\nu/\nu\nu/\gamma + \text{jet}$ we use the gauge-boson masses [54]

$$M_\text{Z} = 91.1876\ \text{GeV}, \quad M_\text{W} = 80.385\ \text{GeV}, \tag{57}$$

and the corresponding widths,

$$\Gamma_\text{Z} = 2.4955\ \text{GeV}, \quad \Gamma_\text{W} = 2.0897\ \text{GeV}. \tag{58}$$

The latter are obtained from state-of-the-art theoretical calculations. For the top-quark [54] and Higgs-boson [47] masses and widths we use

$$m_{\mathrm{t}} = 173.2 \text{ GeV}, \qquad M_{\mathrm{H}} = 125 \text{ GeV}, \tag{59}$$

and[13]

$$\Gamma_{\mathrm{t}} = 1.339 \text{ GeV}, \qquad \Gamma_{\mathrm{H}} = 0 \text{ GeV}. \tag{60}$$

All unstable particles are treated in the complex-mass scheme [55], where width effects are absorbed into the complex-valued renormalised masses

$$\mu_i^2 = M_i^2 - \mathrm{i}\Gamma_i M_i \qquad \text{for } i = \mathrm{W}, \mathrm{Z}, \mathrm{t}. \tag{61}$$

For W+jet and Z+jet production processes the EW couplings are derived from the gauge-boson masses and the Fermi constant, $G_\mu = 1.16637 \times 10^{-5}$ GeV^{-2}, using

$$\alpha = \left| \frac{\sqrt{2} \sin^2 \theta_{\mathrm{w}} \mu_{\mathrm{W}}^2 G_\mu}{\pi} \right|, \tag{62}$$

while for γ+jet production the EW coupling is chosen to be [54]

$$\alpha = \alpha(0) = 1/137.035999074\,. \tag{63}$$

In both schemes the weak mixing angle θ_{w} is determined by

$$\sin^2 \theta_{\mathrm{w}} = 1 - \cos^2 \theta_{\mathrm{w}} = 1 - \frac{\mu_{\mathrm{W}}^2}{\mu_{\mathrm{Z}}^2}, \tag{64}$$

and becomes complex-valued. The G_μ-scheme guarantees an optimal description of pure SU(2) interactions at the EW scale. It is the scheme of choice for W+ jet production, and it provides a very decent description of Z + jet production as well. The $\alpha(0)$ scheme to be used for γ+jet, on the other hand, expresses the fact that on-shell photons effectively couple at a scale Q^2=0 . The CKM matrix is assumed to be diagonal and we checked at LO and NLO QCD that for W+jet production the difference with respect to a non-diagonal CKM matrix is always well below 1%. For the choice of renormalisation and factorisation scales and variations thereof we refer to Section 3.1.

For the calculation of hadron-level cross sections at (N)NLO QCD + (n)NLO EW we employ the `LUXqed_plus_PDF4LHC15_nnlo_100` PDF set, which is based on PDF4LHC NNLO PDFs [35, 56–60] supplemented with QED effects [31]. The same PDF set, and the related α_{S} value, is used throughout, i.e. also in the relevant LO and NLO ingredients used in the estimate of theoretical uncertainties. At the level of precision discussed in this study also the uncertainty on the value of α_{S} becomes relevant. Given 1% uncertainty on the measured value of α_{S} this results in an overall 1–2% normalisation uncertainty on the differential p_{T} distributions. However, one should keep in mind that in the process ratios this uncertainty cancels completely and thus it is irrelevant for background estimates in DM searches at high-MET. Consistently with the five-flavour number scheme employed in the PDFs, b-quarks are treated as massless partons, and channels with initial-state b-quarks are taken into account. All light quarks, including bottom quarks, are treated as massless

[13] Besides loop diagrams with top quarks and Higgs bosons, the NLO EW corrections to $pp \to W^\pm$+jet receive $\mathcal{O}(\alpha^2\alpha_{\mathrm{S}})$ bremsstrahlung contributions from $qb \to q'W^\pm b$ channels that involve s-channel top-quark propagators and thus require a finite top-quark width, for which we use the NLO QCD value $\Gamma_{\mathrm{t}} = 1.339$ GeV. However, at the perturbative order considered in this study, such topologies arise only in QCD–EW interference terms that do not give rise to Breit–Wigner resonances. The dependence of our results on Γ_t is thus completely negligible.

particles, and top-quark loops are included up to NLO throughout. Matrix elements at (N)NLO are evaluated using the five-flavour running of the strong coupling supported by the PDFs and, for consistency, top-quark loops are renormalised in the decoupling scheme. For the NNLO QCD coefficient no top-quark loops are considered.

For the assessment of PDF uncertainties the PDF4LHC prescription [35] is adopted. In addition to standard PDF variations, also additional `LUXqed` variations for the photon PDF are applied.

4.4 Computational frameworks

The NLO QCD and NLO EW calculations for all $pp \to V+\text{jet}$ processes have been performed with Munich+OpenLoops and/or Sherpa+OpenLoops. In these automated frameworks [19, 29, 61] virtual amplitudes are provided by the OpenLoops program [62, 63], combined with the Collier tensor reduction library [64] or with CutTools [65]. The remaining tasks are supported by the two independent and fully automated Monte Carlo generators Munich [66] and Sherpa [67–70]. Additionally, we carefully validated the NLO EW predictions against the results of Refs. [17, 18, 20]. The NLO EW calculations for $pp \to V + 2\,\text{jets}$ performed to test the factorisation of QCD and EW corrections have been checked against the one of Ref. [50] for $pp \to Z + 2\,\text{jets}$ in Ref. [21]. The NLO EW amplitudes for all V+jet processes in OpenLoops have been supplemented with the one- and two-loop analytical Sudakov logarithms of Refs. [22–26].

The NNLO QCD predictions for Z+jet production have been obtained with the parton-level event generator NNLOjet, which provides the necessary infrastructure to perform fully differential calculations at NNLO using the antenna subtraction formalism [71–79]. The computation of $pp \to W$+jet through NNLO is based on the N-jettiness subtraction scheme for NNLO calculations [13]. The above-cut contribution within the N-jettiness subtraction was obtained using Munich+OpenLoops. The NNLO QCD prediction for the $pp \to \gamma$+jet process is based on the calculations of Refs. [15, 16] and has been obtained using MCFM [80]. In order to ensure the correctness of the numerical implementation of cuts and other parameters in the NNLO codes, a detailed comparison has been performed at the level of the NLO QCD results as described above.

5 Summary and conclusions

The precise control of SM backgrounds, and notably of $pp \to Z(\nu\bar{\nu})+\text{jets}$, is crucial in order to maximise the potential of MET+jets searches at the LHC. Such backgrounds can be predicted directly using QCD and EW calculations. Alternatively, QCD and EW calculations can be used to relate them to experimental data for similar processes, e.g. $pp \to \gamma+\text{jets}$, $pp \to W(\ell\nu)+\text{jets}$ and $pp \to Z(\ell^+\ell^-)+\text{jets}$.

In this article we have presented predictions for inclusive vector-boson p_{T} distributions based on the most advanced calculations available today, bringing together results from a number of groups so as to have perturbative QCD to NNLO accuracy, EW corrections to NLO accuracy and additionally the inclusion of 2-loop EW Sudakov logarithms.

A substantial part of our study concerned uncertainty estimates. In particular we proposed and applied various new approaches for uncertainty estimates and correlations across processes and p_{T} regions.

We defined the uncertainties due to normal QCD scale variations in a way that gives a strong correlation across different p_{T} regions, Eq. (15). We then supplemented it with a shape uncertainty that is anti-correlated across p_{T}, Eqs. (17)–(18). To address the long-standing problem of evaluating the correlations between uncertainties for different processes, we separated the uncertainty into process-independent and process-dependent

components. The universal component was taken to be composed of the overall scale and shape uncertainties for the reference $Z+\text{jet}$ process. The process-dependent component, which is generally small, was determined by considering the difference between suitably normalised K-factors for the different processes, Eq. (20). This amounts to a conservative choice of taking the uncertainty on ratios as the difference between the best available prediction and the one at one order lower.

Special attention was devoted to the correlation of $Z/W+\text{jet}$ and $\gamma+\text{jet}$ production. In that case a substantial non-universal contribution is associated with the masslessness of the photon and the need to control collinear divergent $q \to q\gamma$ radiation through a photon-isolation prescription. We introduced a novel photon-isolation prescription with a dynamically chosen isolation radius, Eq. (51), designed to suppress $q \to \gamma q$ radiative effects in a way that is similar to the effect of the masses of the Z and W bosons in the case of $q \to Vq$ splittings at large p_{T}. Such a dynamic isolation allows one to split γ+jet production into a quasi-universal part, which can be treated on the same footing as $Z+\text{jet}$ and $W+\text{jet}$ production, and a non-universal part which is kept uncorrelated. The non-universal part is given by the difference between the cross sections with conventional and dynamic photon isolation prescriptions.

For pure EW corrections we considered three uncertainty sources for unknown higher order contributions. These address unknown Sudakov logarithms beyond NNLO and/or NLL accuracy, as well as unknown hard (non-Sudakov) EW corrections beyond NLO and process-correlation effects.

One potentially large source of uncertainty arises from mixed QCD and EW corrections, given that both NLO α_{S} and NLO α corrections can be large and that the NNLO $\alpha\alpha_{\mathrm{S}}$ contributions are not currently known. We chose a multiplicative scheme for combining EW and QCD corrections. To obtain an estimate of unknown $\mathcal{O}(\alpha\alpha_{\mathrm{S}})$ contributions not captured by this factorised ansatz, we studied the NLO EW corrections to $V+2\,\text{jet}$ production, which represent the real-virtual part of a full $\mathcal{O}(\alpha\alpha_{\mathrm{S}})$ calculation for $V+\text{jet}$ production. Based on this analysis, we concluded that it is reasonable to assume that the multiplicative combination of QCD and EW corrections describes the full $\mathcal{O}(\alpha\alpha_{\mathrm{S}})$ contribution with a relative uncertainty of 10%.

Overall, QCD corrections are substantial, a few tens of percent at NLO, and up to 10% at NNLO. The NNLO results are consistent with the NLO predictions within our prescription for the uncertainty bands of the latter. This is true not just for absolute cross sections and their shapes, but also for ratios of cross sections. These ratios are remarkably stable across LO, NLO and NNLO QCD corrections, see Figure 4. Using dynamic isolation, this statement holds true also for the $\gamma+\text{jet}$ process at $p_{\mathrm{T}} \gtrsim 300$ GeV.

The EW corrections to V+jet cross sections amount to a few tens of percent in the TeV region, see Figure 6. In the ratios they cancel only in part, due to the sensitivity of EW effects to the SU(2) charges of the produced vector bosons. At the TeV scale, the NNLO Sudakov logarithms can reach the several percent level and their systematic inclusion is an important ingredient in order to achieve percent precision at very high p_{T}.

In Figure 17 we summarize our uncertainty estimates for the different V+jet processes and process ratios. Here we combine in quadrature all sources of perturbative uncertainties at NLO QCD $\otimes$ nNLO EW and we overlay the remaining PDF uncertainties. The impact of NNLO QCD corrections and NNLO QCD scale uncertainties are also shown. The nominal p_{T} distributions at NLO QCD $\otimes$ nNLO EW are constrained at the 10% level up to about 1 TeV and at the 20% level up to about 2 TeV. In the process ratios these uncertainties cancel to a large extent. In particular, in the Z/W ratio remaining uncertainties are at the level of only 1–2% up to 1 TeV and below 5% up to 2 TeV. Similarly, the Z/γ ratio is constrained at the 5% level up to 2 TeV. Noteworthy, including the NNLO QCD corrections the process ratios remain very stable and in particular within the uncertainty estimates

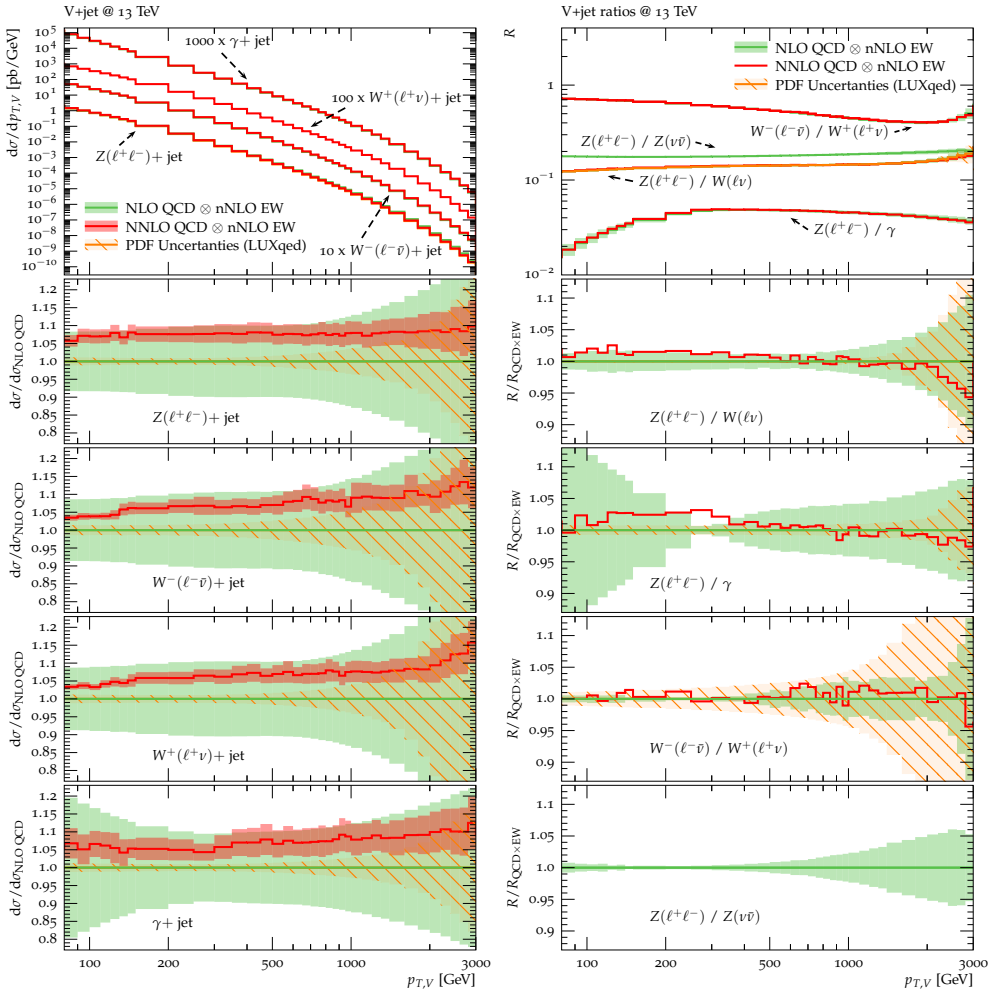

Figure 17: Predictions at NLO QCD ⊗ nNLO EW and NNLO QCD ⊗ nNLO EW for $V+$jet spectra (left) and ratios (right) at 13 TeV. The lower frames show the relative impact of NNLO corrections and theory uncertainties normalised to NLO QCD ⊗ nNLO EW. The green bands at NLO QCD ⊗ nNLO EW correspond to the combination (in quadrature) of the perturbative QCD, EW and mixed QCD-EW uncertainties, according to Eq. (45), while the NNLO QCD ⊗ nNLO EW bands (red) display only QCD scale variations. PDF uncertainties are shown as separate hashed orange bands.

based on NLO QCD. PDF uncertainties are below the perturbative uncertainties in all nominal distributions and all but the W^-/W^+ ratio. Clearly, a precise measurement of the W^-/W^+ ratio at high p_{T}, where perturbative uncertainties almost completely cancel, will help to improve PDF fits.

Our predictions are provided in the form of tables for the central predictions and for the different uncertainty sources. Each uncertainty source is to be treated as a 1-standard deviation uncertainty and pragmatically associated with a Gaussian-distributed nuisance parameter.

The predictions are given at parton level as distributions of the vector boson p_{T}, with loose cuts and inclusively over other radiation. They are intended to be propagated to an experimental analysis using Monte Carlo parton shower samples whose inclusive vector-boson p_{T} distribution has been reweighted to agree with our parton-level predictions. The impact of additional cuts, non-perturbative effects on lepton isolation, etc., can then be deduced from the Monte Carlo samples. The additional uncertainties associated with the

Monte Carlo simulation are expected to be relatively small, insofar as the vector-boson p_{T} distribution that we calculate is closely connected to the main experimental observables used in MET+jets searches.

Some caution is needed in implementing the results of this paper: for example the uncertainty prescriptions are tied to the use of the central values that we provide. If an experiment relies on central values that differ, e.g. through the use of MC samples that are not reweighted to our nominal predictions, then the uncertainty scheme that we provide may no longer be directly applicable. Furthermore, for searches that rely on features of the event other than missing transverse momentum, one should be aware that our approach might need to be extended. This would be the case notably for any observable that relies directly on jet observables, whether related to the recoiling jet or vetoes on additional jets.

Overall, it is possible to obtain precise theoretical control both for vector-boson p_{T} distributions, and for their ratios, at the level of a few percent. We expect this precision, across a wide range of p_{T}, to be of significant benefit in MET+jets searches, notably enabling reliable identification or exclusion of substantially smaller BSM signals than was possible so far.

Note added

This preprint was released as a reference for dark matter searches presented at LHCP 2017. While the effect of the recently computed NNLO QCD corrections is illustrated in various figures, in order to reflect the usage of our calculations in present experimental analysis, only NLO QCD and nNLO EW effects have been propagated through our framework of uncertainty estimates. An update of this study, with a full NNLO treatment of uncertainties, will be released in the near future.

Acknowledgments

We wish to thank Frank Krauss, Keith Ellis, Christian Gütschow, Sarah Malik, Fabio Maltoni, Holger Schulz and Graeme Watt for valuable discussions. This research was supported in part by the UK Science and Technology Facilities Council, the Swiss National Science Foundation (SNF) under contracts 200020-162487, CRSII2-160814, and BSCGI0-157722, and by the Research Executive Agency (REA) of the European Union under the Grant Agreements PITN-GA-2012-316704 ("HiggsTools"), PITN–GA–2012–315877 ("MCnet"), and the ERC Advanced Grants MC@NNLO (340983) and LHCtheory (291377). R.B. is supported by the DOE contract DE-AC02-06CH11357. F.P. is supported by the DOE grants DE-FG02- 91ER40684 and DE-AC02-06CH11357. C.W. is supported by the National Science Foundation through award number PHY-1619877. The research of J.M.C. is supported by the US DOE under contract DE-AC02-07CH11359. The work of S.D. is supported by the German Federal Ministry for Education and Research (BMBF). This research used resources of the Argonne Leadership Computing Facility, which is a DOE Office of Science User Facility supported under Contract DE-AC02-06CH11357. We also acknowledge support provided by the Center for Computational Research at the University at Buffalo and the Wilson HPC Computing Facility at Fermilab.

A Theoretical predictions and uncertainties

Predictions for the various $pp \to V+\text{jet}$ processes listed in Table 2 with $\sqrt{s} = 13$ TeV are provided at `http://lpcc.web.cern.ch/LPCC/index.php?page=dm_wg_docs` The various predictions and related uncertainties at the highest available perturbative order and the labels of the corresponding histograms are listed in Table 3. At present data files are available at NLO QCD and nNLO EW for all processes. NNLO QCD data files will be made available in the near future. Table 3 also lists the additionally available building blocks for the construction of the uncertainties at the various perturbative orders. Results for p_{T} distributions are given in pb/GeV.

All ingredients and related uncertainties should be combined as indicated in Eq. (42) and Eq. (45), and we recall that all nuisance parameters in Eq. (45) should be Gaussian distributed with one standard deviation corresponding to the range $[-1, +1]$ for all $\varepsilon_{\mathrm{QCD},i}$, $\varepsilon_{\mathrm{EW},i}$ and $\varepsilon_{\mathrm{mix}}$.

All predictions and uncertainties for $pp \to \gamma+\text{jet}$ are based on the dynamic photon isolation prescription introduced in Section 4.1. As explained therein, this requires an extra $\gamma+$ jet specific uncertainty, which needs to be evaluated by means of a separate reweighting in a standard Frixione isolation setup with fixed cone. Corresponding theoretical predictions are denoted as $K_{\mathrm{NLO}}^{(\gamma,\mathrm{fix})}(x)$ in Table 3.

B QCD and EW uncertainties

In this appendix we present a series of technical plots that illustrate the relative importance of the various sources of QCD and EW uncertainties discussed in Sections 3.1–3.2. The impact of individual QCD uncertainties, $\delta^{(i)}K_{\mathrm{N}^k\mathrm{LO}}$, in p_{T} spectra and ratios is illustrated in Figures 18–19. Similar plots for the three types of EW uncertainties, $\delta^{(i)}\kappa_{\mathrm{EW}}^{(V)}$, are shown in Figures 20–21.

process	QCD order	EW order	label
$pp \to \ell^+\nu_\ell/\ell^-\bar{\nu}_\ell + \text{jet}$	NLO QCD	nNLO EW	evj
$pp \to \nu_\ell\bar{\nu}_\ell + \text{jet}$	NLO QCD	nNLO EW	vvj
$pp \to \ell^+\ell^- + \text{jet}$	NLO QCD	nNLO EW	eej
$pp \to \gamma + \text{jet}$	NLO QCD	nNLO EW	aj

Table 2: List of processes, highest available QCD and EW order, and process labels used in data files (see Table 3).

prediction	equation	label	correlation
$\frac{\mathrm{d}}{\mathrm{d}x}\sigma^{(V)}_{\mathrm{LO\,QCD}}(\vec{\mu}_0)$ [pb/GeV]	(21)	proc_x_LO	-
$K^{(V)}_{\mathrm{LO}}(x)$	(21)	proc_x_K_LO	-
$K^{(V)}_{\mathrm{NLO}}(x)$	(21),(14)	proc_x_K_NLO	-
$K^{(\gamma,\mathrm{fix})}_{\mathrm{NLO}}(x)$	(21),(14),(54)	aj_x_K_NLO_fix	-
$\delta^{(1)}K^{(V)}_{\mathrm{NLO}}(x)$	(21),(15)	proc_x_d1K_NLO	yes
$\delta^{(2)}K^{(V)}_{\mathrm{NLO}}(x)$	(21), (17)	proc_x_d2K_NLO	yes
$\delta^{(3)}K^{(V)}_{\mathrm{NLO}}(x)$	(21), (20)	proc_x_d3K_NLO	yes
$\kappa^{(V)}_{\mathrm{nNLO\,EW}}(x)$	(25), (39)	proc_x_kappa_EW	-
$\delta^{(1)}\kappa^{(V)}_{\mathrm{nNLO\,EW}}(x)$	(33), (39)	proc_x_d1kappa_EW	yes
$\delta^{(2)}\kappa^{(V)}_{\mathrm{nNLO\,EW}}(x)$	(34), (39)	proc_x_d2kappa_EW	no
$\delta^{(3)}\kappa^{(V)}_{\mathrm{nNLO\,EW}}(x)$	(37), (39)	proc_x_d3kappa_EW	no
$\delta K^{(V)}_{\mathrm{mix}}(x)$	(46)	proc_x_dK_NLO_mix	yes
$\frac{\mathrm{d}}{\mathrm{d}x}\sigma^{(V)}_{\mathrm{LO}\,\gamma-\mathrm{ind.}}$ [pb/GeV]	(7)	proc_x_gammaind_LO	-
$\delta^{(1)}K^{(V)}_{\mathrm{LO}}(x)$	(21),(15)	proc_x_d1K_LO	yes
$\delta^{(2)}K^{(V)}_{\mathrm{LO}}(x)$	(21), (17)	proc_x_d2K_LO	yes
$\kappa^{(V)}_{\mathrm{NLO\,EW}}(x)$	(39)	proc_x_kappa_NLO_EW	-
$\kappa^{(V)}_{\mathrm{NNLO\,Sud}}(x)$	(39)	proc_x_kappa_NNLO_Sud	-

Table 3: Naming scheme for the theoretical predictions and uncertainties described in Section 3. The upper part lists the highest available perturbation order, while the predictions in the lower part are included for completeness. The last column indicates the correlation of the uncertainties across different V+jets processes. The actual distribution names are x=pTV and the individual processes are available in the files proc.dat with process names proc=eej,vvj,evj,aj, as defined in Table 2. Absolute predictions for p_{T} distributions are in pb/GeV.

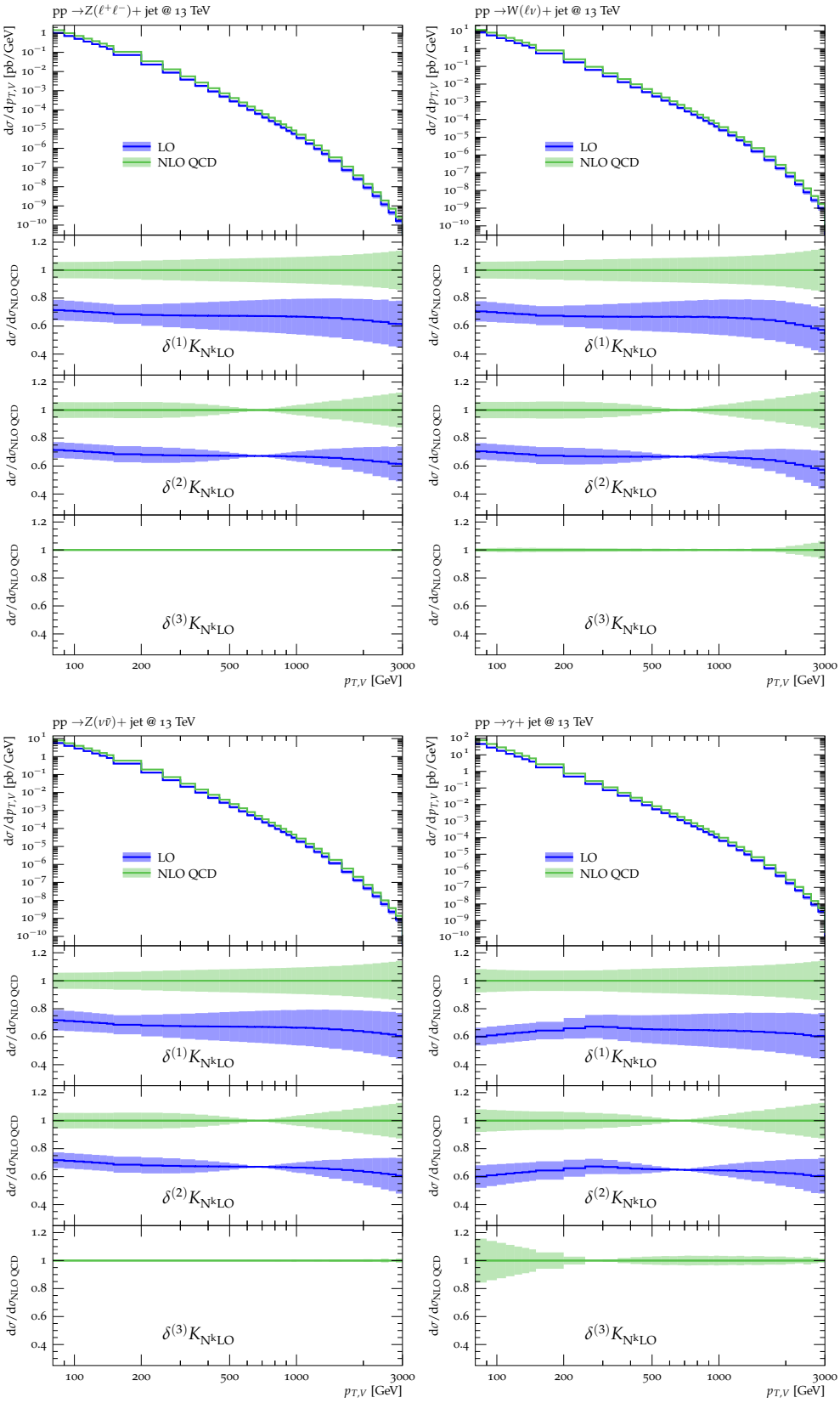

Figure 18: Higher-order QCD predictions and uncertainties for various $pp \to V$+jet processes at 13 TeV. Absolute predictions at LO and NLO QCD are displayed in the main frame. In the ratio plots all results are normalised to NLO QCD, and the bands correspond to the three types of QCD uncertainties, $\delta^{(i)} K_{\mathrm{N}^k\mathrm{LO}}$, i.e. scale uncertainties (15), shape uncertainties (17) and process-correlation uncertainties (20).

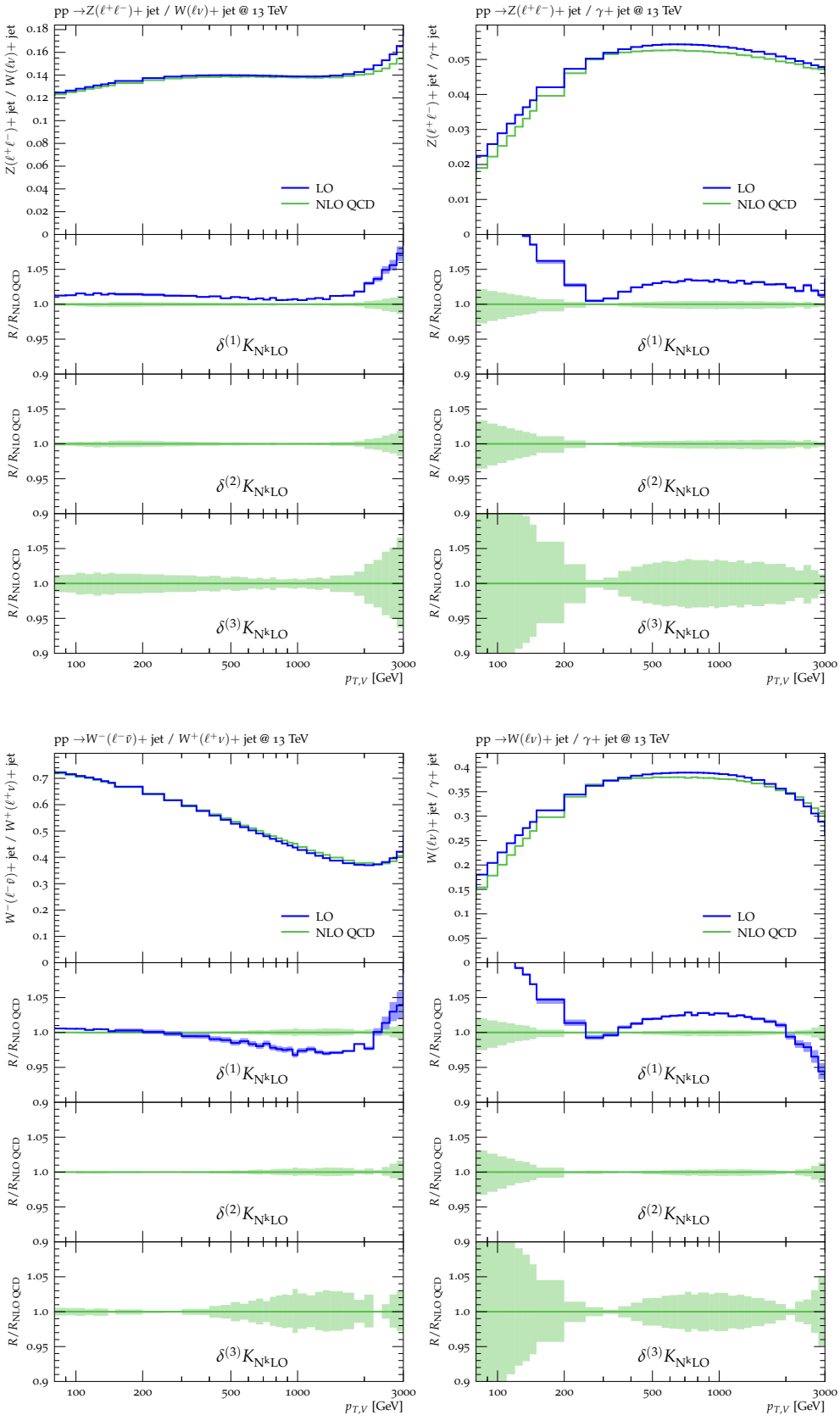

Figure 19: Ratios of p_{T}-distributions for various $pp \to V+$jet processes at LO and NLO QCD. The related scale uncertainties (15), shape uncertainties (17) and process-correlation uncertainties (20) are correlated amongst all processes.

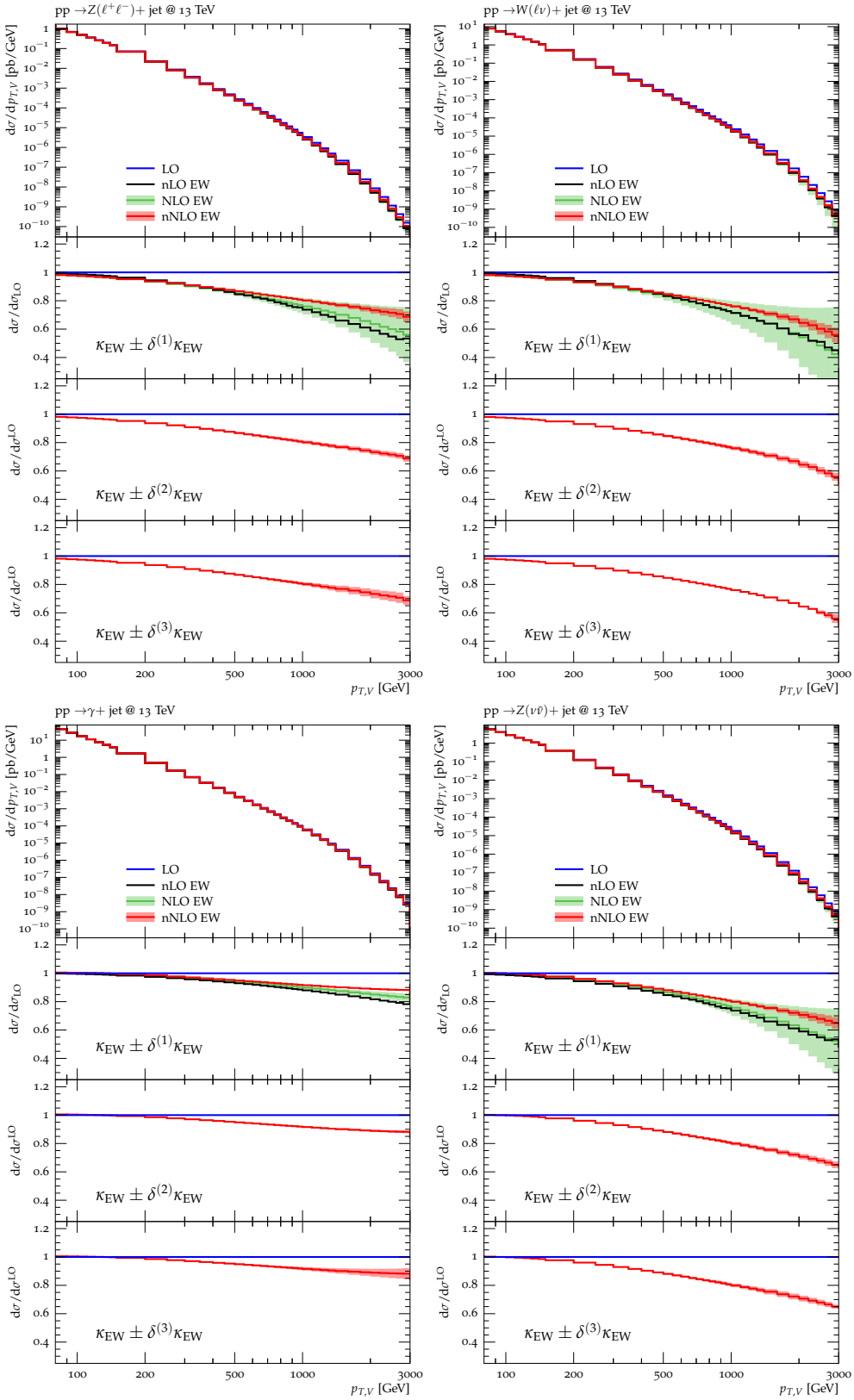

Figure 20: Higher-order EW predictions and uncertainties for different $pp \to V+\text{jet}$ processes at 13 TeV. The main frames display absolute predictions at LO (blue), NLO EW (green) and nNLO EW (red), as well as NLL Sudakov logarithms at NLO (black). The latter are dubbed nLO EW. In the ratio plots all results are normalised to LO. The bands correspond to the three types of EW uncertainties, $\delta^{(i)}\kappa_{\text{EW}}^{(V)}$. At nNLO EW (red bands) they are defined in Eqs. (33), (34) and (37), while at NLO EW (green band) only the uncertainty $\delta^{(1)}\kappa_{\text{NLO EW}}^{(V)}$, defined in Eq. (38), is plotted.

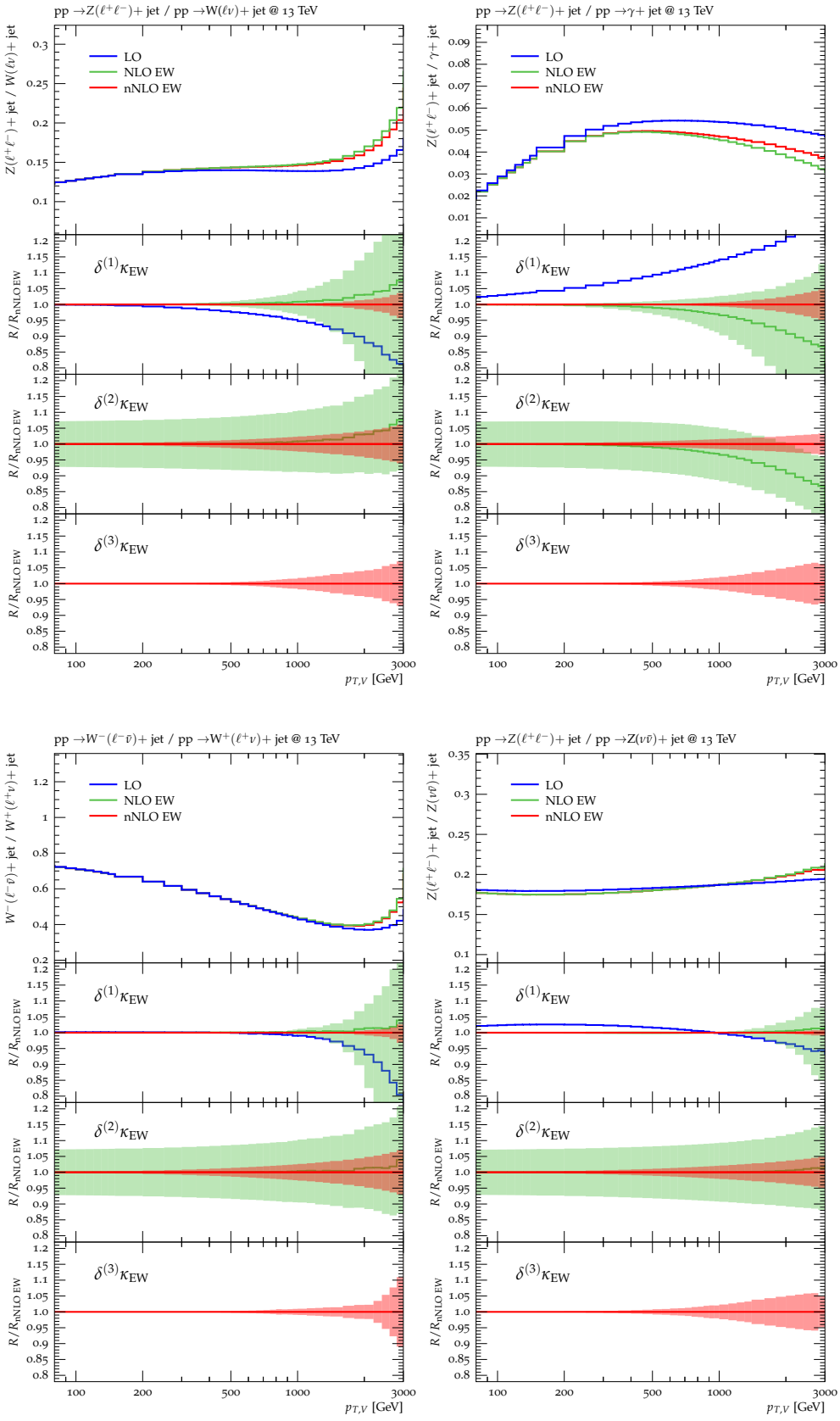

Figure 21: Ratios of p_{T}-distributions for various $pp \to V+$jet processes at LO, NLO EW and nNLO EW. The related EW uncertainties, $\delta^{(i)}\kappa_{\mathrm{EW}}^{(V)}$, are defined in Eqs. (33), (34) and (37) at nNLO and in Eq. (38) at NLO. The uncertainty $\delta^{(1)}\kappa_{\mathrm{EW}}^{(V)}$ is correlated amongst processes, while $\delta^{(2)}\kappa_{\mathrm{EW}}^{(V)}$ and $\delta^{(3)}\kappa_{\mathrm{EW}}^{(V)}$ are uncorrelated.

References

[1] Z. Bern, G. Diana, L. J. Dixon, F. Febres Cordero, S. Hoche, H. Ita et al., *Driving Missing Data at Next-to-Leading Order*, *Phys. Rev.* **D84** (2011) 114002, [1106.1423].

[2] S. Ask, M. A. Parker, T. Sandoval, M. E. Shea and W. J. Stirling, *Using gamma+jets Production to Calibrate the Standard Model Z(nunu)+jets Background to New Physics Processes at the LHC*, *JHEP* **10** (2011) 058, [1107.2803].

[3] S. A. Malik and G. Watt, *Ratios of W and Z Cross Sections at Large Boson p_T as a Constraint on PDFs and Background to New Physics*, *JHEP* **02** (2014) 025, [1304.2424].

[4] D. Abercrombie et al., *Dark Matter Benchmark Models for Early LHC Run-2 Searches: Report of the ATLAS/CMS Dark Matter Forum*, 1507.00966.

[5] ATLAS collaboration, M. Aaboud et al., *Search for new phenomena in final states with an energetic jet and large missing transverse momentum in pp collisions at $\sqrt{s} = 13$ TeV using the ATLAS detector*, *Phys. Rev.* **D94** (2016) 032005, [1604.07773].

[6] CMS collaboration, V. Khachatryan et al., *Search for dark matter in proton-proton collisions at 8 TeV with missing transverse momentum and vector boson tagged jets*, *JHEP* **12** (2016) 083, [1607.05764].

[7] CMS collaboration, A. M. Sirunyan et al., *Search for dark matter produced with an energetic jet or a hadronically decaying W or Z boson at $\sqrt{s} = 13$ TeV*, 1703.01651.

[8] A. Gehrmann-De Ridder, T. Gehrmann, E. W. N. Glover, A. Huss and T. A. Morgan, *Precise QCD predictions for the production of a Z boson in association with a hadronic jet*, *Phys. Rev. Lett.* **117** (2016) 022001, [1507.02850].

[9] A. Gehrmann-De Ridder, T. Gehrmann, E. W. N. Glover, A. Huss and T. A. Morgan, *The NNLO QCD corrections to Z boson production at large transverse momentum*, *JHEP* **07** (2016) 133, [1605.04295].

[10] A. Gehrmann-De Ridder, T. Gehrmann, E. W. N. Glover, A. Huss and T. A. Morgan, *NNLO QCD corrections for Drell-Yan p_T^Z and ϕ^* observables at the LHC*, *JHEP* **11** (2016) 094, [1610.01843].

[11] R. Boughezal, J. M. Campbell, R. K. Ellis, C. Focke, W. T. Giele, X. Liu et al., *Z-boson production in association with a jet at next-to-next-to-leading order in perturbative QCD*, *Phys. Rev. Lett.* **116** (2016) 152001, [1512.01291].

[12] R. Boughezal, X. Liu and F. Petriello, *Phenomenology of the Z-boson plus jet process at NNLO*, *Phys. Rev.* **D94** (2016) 074015, [1602.08140].

[13] R. Boughezal, C. Focke, X. Liu and F. Petriello, *W-boson production in association with a jet at next-to-next-to-leading order in perturbative QCD*, *Phys. Rev. Lett.* **115** (2015) 062002, [1504.02131].

[14] R. Boughezal, X. Liu and F. Petriello, *W-boson plus jet differential distributions at NNLO in QCD*, *Phys. Rev.* **D94** (2016) 113009, [1602.06965].

[15] J. M. Campbell, R. K. Ellis and C. Williams, *Direct photon production at next-to-next-to-leading order*, 1612.04333.

[16] J. M. Campbell, R. K. Ellis and C. Williams, *Driving Miss Data: Going Up a Gear to NNLO*, 1703.10109.

[17] A. Denner, S. Dittmaier, T. Kasprzik and A. Mück, *Electroweak corrections to dilepton + jet production at hadron colliders*, *JHEP* **06** (2011) 069, [1103.0914].

[18] A. Denner, S. Dittmaier, T. Kasprzik and A. Mück, *Electroweak corrections to monojet production at the LHC*, *Eur. Phys. J.* **C73** (2013) 2297, [1211.5078].

[19] S. Kallweit, J. M. Lindert, P. Maierhoefer, S. Pozzorini and M. Schoenherr, *NLO QCD+EW predictions for V + jets including off-shell vector-boson decays and multijet merging*, *JHEP* **04** (2016) 021, [1511.08692].

[20] A. Denner, S. Dittmaier, T. Kasprzik and A. Mück, *Electroweak corrections to W + jet hadroproduction including leptonic W-boson decays*, *JHEP* **08** (2009) 075, [0906.1656].

[21] J. R. Andersen et al., *Les Houches 2015: Physics at TeV Colliders Standard Model Working Group Report*, in *9th Les Houches Workshop on Physics at TeV Colliders (PhysTeV 2015) Les Houches, France, June 1-19, 2015*, 2016. 1605.04692.

[22] J. H. Kühn, A. Kulesza, S. Pozzorini and M. Schulze, *Logarithmic electroweak corrections to hadronic Z+1 jet production at large transverse momentum*, *Phys. Lett.* **B609** (2005) 277–285, [hep-ph/0408308].

[23] J. H. Kühn, A. Kulesza, S. Pozzorini and M. Schulze, *Electroweak corrections to hadronic photon production at large transverse momenta*, *JHEP* **03** (2006) 059, [hep-ph/0508253].

[24] J. H. Kühn, A. Kulesza, S. Pozzorini and M. Schulze, *One-loop weak corrections to hadronic production of Z bosons at large transverse momenta*, *Nucl. Phys.* **B727** (2005) 368–394, [hep-ph/0507178].

[25] J. H. Kühn, A. Kulesza, S. Pozzorini and M. Schulze, *Electroweak corrections to large transverse momentum production of W bosons at the LHC*, *Phys. Lett.* **B651** (2007) 160–165, [hep-ph/0703283].

[26] J. H. Kühn, A. Kulesza, S. Pozzorini and M. Schulze, *Electroweak corrections to hadronic production of W bosons at large transverse momenta*, *Nucl. Phys.* **B797** (2008) 27–77, [0708.0476].

[27] R. Boughezal, A. Guffanti, F. Petriello and M. Ubiali, *The impact of the LHC Z-boson transverse momentum data on PDF determinations*, 1705.00343.

[28] B. Jantzen, J. H. Kuhn, A. A. Penin and V. A. Smirnov, *Two-loop electroweak logarithms in four-fermion processes at high energy*, *Nucl. Phys.* **B731** (2005) 188–212, [hep-ph/0509157].

[29] S. Kallweit, J. M. Lindert, P. Maierhoefer, S. Pozzorini and M. Schoenherr, *NLO electroweak automation and precise predictions for W+multijet production at the LHC*, *JHEP* **04** (2015) 012, [1412.5157].

[30] C. Schmidt, J. Pumplin, D. Stump and C. P. Yuan, *CT14QED parton distribution functions from isolated photon production in deep inelastic scattering*, *Phys. Rev.* **D93** (2016) 114015, [1509.02905].

[31] A. Manohar, P. Nason, G. P. Salam and G. Zanderighi, *How bright is the proton? A precise determination of the photon parton distribution function*, *Phys. Rev. Lett.* **117** (2016) 242002, [1607.04266].

[32] NNPDF collaboration, R. D. Ball et al., *Parton distributions with QED corrections*, *Nucl.Phys.* **B877** (2013) 290–320, [1308.0598].

[33] V. Bertone and S. Carrazza, *Combining NNPDF3.0 and NNPDF2.3QED through the APFEL evolution code*, *PoS* **DIS2016** (2016) 031.

[34] D. de Florian, G. F. R. Sborlini and G. Rodrigo, *QED corrections to the Altarelli-Parisi splitting functions*, *Eur. Phys. J.* **C76** (2016) 282, [1512.00612].

[35] J. Butterworth et al., *PDF4LHC recommendations for LHC Run II*, *J. Phys.* **G43** (2016) 023001, [1510.03865].

[36] W.-H. Li, R.-Y. Zhang, W.-G. Ma, L. Guo, X.-Z. Li and Y. Zhang, *NLO QCD and electroweak corrections to WW+jet production with leptonic W -boson decays at LHC*, *Phys. Rev.* **D92** (2015) 033005, [1507.07332].

[37] Y. Wang, R.-Y. Zhang, W.-G. Ma, X.-Z. Li and L. Guo, *QCD and electroweak corrections to ZZ+jet production with Z -boson leptonic decays at the LHC*, *Phys. Rev.* **D94** (2016) 013011, [1604.04080].

[38] J. M. Campbell, R. K. Ellis and G. Zanderighi, *Next-to-leading order predictions for $WW + 1$ jet distributions at the LHC*, *JHEP* **12** (2007) 056, [0710.1832].

[39] S. Dittmaier, S. Kallweit and P. Uwer, *NLO QCD corrections to WW+jet production at hadron colliders*, *Phys. Rev. Lett.* **100** (2008) 062003, [0710.1577].

[40] S. Dittmaier, S. Kallweit and P. Uwer, *NLO QCD corrections to pp/ppbar –> WW+jet+X including leptonic W-boson decays*, *Nucl. Phys.* **B826** (2010) 18–70, [0908.4124].

[41] T. Binoth, T. Gleisberg, S. Karg, N. Kauer and G. Sanguinetti, *NLO QCD corrections to ZZ+ jet production at hadron colliders*, *Phys. Lett.* **B683** (2010) 154–159, [0911.3181].

[42] F. Campanario, C. Englert, M. Spannowsky and D. Zeppenfeld, *NLO-QCD corrections to W gamma j production*, *Europhys. Lett.* **88** (2009) 11001, [0908.1638].

[43] F. Campanario, C. Englert, S. Kallweit, M. Spannowsky and D. Zeppenfeld, *NLO QCD corrections to WZ+jet production with leptonic decays*, *JHEP* **07** (2010) 076, [1006.0390].

[44] F. Cascioli, S. Höche, F. Krauss, P. Maierhöfer, S. Pozzorini and F. Siegert, *Precise Higgs-background predictions: merging NLO QCD and squared quark-loop corrections to four-lepton + 0,1 jet production*, *JHEP* **01** (2014) 046, [1309.0500].

[45] J. M. Campbell, D. J. Miller and T. Robens, *Next-to-Leading Order Predictions for WW+Jet Production*, *Phys. Rev.* **D92** (2015) 014033, [1506.04801].

[46] LHC Higgs Cross Section Working Group collaboration, S. Dittmaier et al., *Handbook of LHC Higgs Cross Sections: 2. Differential Distributions*, 1201.3084.

[47] LHC Higgs Cross Section Working Group collaboration, S. Heinemeyer et al., *Handbook of LHC Higgs Cross Sections: 3. Higgs Properties*, 1307.1347.

[48] LHC Higgs Cross Section Working Group collaboration, D. de Florian et al., *Handbook of LHC Higgs Cross Sections: 4. Deciphering the Nature of the Higgs Sector*, 1610.07922.

[49] M. Rubin, G. P. Salam and S. Sapeta, *Giant QCD K-factors beyond NLO*, *JHEP* **09** (2010) 084, [1006.2144].

[50] A. Denner, L. Hofer, A. Scharf and S. Uccirati, *Electroweak corrections to lepton pair production in association with two hard jets at the LHC*, *JHEP* **01** (2015) 094, [1411.0916].

[51] S. Frixione, *Isolated photons in perturbative QCD*, *Phys. Lett.* **B429** (1998) 369–374, [hep-ph/9801442].

[52] CMS collaboration, V. Khachatryan et al., *Comparison of the Z/γ + jets to γ + jets cross sections in pp collisions at $\sqrt{s} = 8$ TeV*, *JHEP* **10** (2015) 128, [1505.06520].

[53] A. Karlberg, E. Re and G. Zanderighi, *NNLOPS accurate Drell-Yan production*, *JHEP* **09** (2014) 134, [1407.2940].

[54] Particle Data Group collaboration, K. Olive et al., *Review of Particle Physics*, *Chin.Phys.* **C38** (2014) 090001.

[55] A. Denner et al., *Electroweak corrections to charged-current $e^+e^- \to 4$ fermion processes: Technical details and further results*, *Nucl.Phys.* **B724** (2005) 247–294, [hep-ph/0505042].

[56] NNPDF collaboration, R. D. Ball et al., *Parton distributions for the LHC Run II*, *JHEP* **04** (2015) 040, [1410.8849].

[57] S. Dulat, T.-J. Hou, J. Gao, M. Guzzi, J. Huston, P. Nadolsky et al., *New parton distribution functions from a global analysis of quantum chromodynamics*, *Phys. Rev.* **D93** (2016) 033006, [1506.07443].

[58] L. A. Harland-Lang, A. D. Martin, P. Motylinski and R. S. Thorne, *Parton distributions in the LHC era: MMHT 2014 PDFs*, *Eur. Phys. J.* **C75** (2015) 204, [1412.3989].

[59] J. Gao and P. Nadolsky, *A meta-analysis of parton distribution functions*, *JHEP* **07** (2014) 035, [1401.0013].

[60] S. Carrazza, S. Forte, Z. Kassabov, J. I. Latorre and J. Rojo, *An Unbiased Hessian Representation for Monte Carlo PDFs*, *Eur. Phys. J.* **C75** (2015) 369, [1505.06736].

[61] S. Kallweit, J. M. Lindert, S. Pozzorini and M. Schonherr, *NLO QCD+EW predictions for $2\ell 2\nu$ diboson signatures at the LHC*, 1705.00598.

[62] F. Cascioli, J. M. Lindert, P. Maierhöfer and S. Pozzorini, *The* OpenLoops *one-loop generator*, *publicly available at* `http://openloops.hepforge.org` .

[63] F. Cascioli, P. Maierhöfer and S. Pozzorini, *Scattering Amplitudes with Open Loops*, *Phys.Rev.Lett.* **108** (2012) 111601, [1111.5206].

[64] A. Denner, S. Dittmaier and L. Hofer, *Collier: a fortran-based Complex One-Loop LIbrary in Extended Regularizations*, *Comput. Phys. Commun.* **212** (2017) 220–238, [1604.06792].

[65] G. Ossola, C. G. Papadopoulos and R. Pittau, *CutTools: A Program implementing the OPP reduction method to compute one-loop amplitudes*, *JHEP* **03** (2008) 042, [0711.3596].

[66] S. Kallweit, MUNICH: *"MUlti-chaNnel Integrator at Swiss (CH) precision", an automated parton level NLO generator. In preparation* .

[67] T. Gleisberg, S. Hoeche, F. Krauss, M. Schonherr, S. Schumann, F. Siegert et al., *Event generation with SHERPA 1.1*, *JHEP* **02** (2009) 007, [0811.4622].

[68] F. Krauss, R. Kuhn and G. Soff, *AMEGIC++ 1.0: A Matrix element generator in C++*, *JHEP* **02** (2002) 044, [hep-ph/0109036].

[69] T. Gleisberg and F. Krauss, *Automating dipole subtraction for QCD NLO calculations*, *Eur. Phys. J.* **C53** (2008) 501–523, [0709.2881].

[70] M. Schönherr *In preparation* .

[71] A. Gehrmann-De Ridder, T. Gehrmann and E. W. N. Glover, *Antenna subtraction at NNLO*, *JHEP* **09** (2005) 056, [hep-ph/0505111].

[72] A. Gehrmann-De Ridder, T. Gehrmann and E. W. N. Glover, *Gluon-gluon antenna functions from Higgs boson decay*, *Phys. Lett.* **B612** (2005) 49–60, [hep-ph/0502110].

[73] A. Gehrmann-De Ridder, T. Gehrmann and E. W. N. Glover, *Quark-gluon antenna functions from neutralino decay*, *Phys. Lett.* **B612** (2005) 36–48, [hep-ph/0501291].

[74] A. Daleo, T. Gehrmann and D. Maitre, *Antenna subtraction with hadronic initial states*, *JHEP* **04** (2007) 016, [hep-ph/0612257].

[75] A. Daleo, A. Gehrmann-De Ridder, T. Gehrmann and G. Luisoni, *Antenna subtraction at NNLO with hadronic initial states: initial-final configurations*, *JHEP* **01** (2010) 118, [0912.0374].

[76] T. Gehrmann and P. F. Monni, *Antenna subtraction at NNLO with hadronic initial states: real-virtual initial-initial configurations*, *JHEP* **12** (2011) 049, [1107.4037].

[77] R. Boughezal, A. Gehrmann-De Ridder and M. Ritzmann, *Antenna subtraction at NNLO with hadronic initial states: double real radiation for initial-initial configurations with two quark flavours*, *JHEP* **02** (2011) 098, [1011.6631].

[78] A. Gehrmann-De Ridder, T. Gehrmann and M. Ritzmann, *Antenna subtraction at NNLO with hadronic initial states: double real initial-initial configurations*, *JHEP* **10** (2012) 047, [1207.5779].

[79] J. Currie, E. W. N. Glover and S. Wells, *Infrared Structure at NNLO Using Antenna Subtraction*, *JHEP* **04** (2013) 066, [1301.4693].

[80] R. Boughezal, J. M. Campbell, R. K. Ellis, C. Focke, W. Giele, X. Liu et al., *Color singlet production at NNLO in MCFM*, *Eur. Phys. J.* **C77** (2017) 7, [1605.08011].